Master Thesis

Electrical Engineering

Thesis number:

August, 2012

Oil Well Monitoring by Ultra-wideband Ground Penetrating Synthetic Aperture Radar

Daniel Oloumi

This thesis is presented as part of Degree of
Master of Science in Electrical Engineering with emphasis on Radio Communication

Blekinge Institute of Technology (BTH)
August 2012

School of Engineering
Department of Electrical Engineering
Blekinge Institute of Technology, Sweden

Supervisor: Prof. Mats Pettersson

This thesis is submitted to the School of Engineering at Blekinge Institute of Technology in partial fulfillment of the requirements for the degree of Master of Science in Electrical Engineering with emphasis on Radio Communications. The thesis is equivalent to twenty weeks of full time studies.

Contact Information:

Author:
Daniel Oloumi
Email: daob10@student.bth.se
oloumi@ualberta.ca

University Supervisor:
Prof. Mats Pettersson
School of Engineering
Blekinge Institute of Technology (BTH), Sweden.
E-mail: mats.pettersson@bth.se

University Co-supervisor:
Dr. Pedram Mousavi
Dept. of Electrical Engineering, University of Alberta
University of Alberta, Canada.
E-mail: pmousavi@ualberta.ca

University Co-supervisor:
Prof. Duncan Elliot
Dept. of Electrical Engineering, University of Alberta
University of Alberta, Canada.
E-mail: Duncan.Elliott@ualberta.ca

ABSTRACT

Radar has been used for remote sensing and surveillance for decades. Nowadays radar remote sensing and radar surveillance is used for many different things in the modern society. Radar can sense objects or environments from very long distance. Electromagnetic radar waves can work where and when light cannot. This unique ability of radar made remote sensing techniques available in research and in industrial applications. Radar can operate in any climate and any time of the day. Using ultra-wideband (UWB) pulses for radar in combination with synthesizing apertures, which is so called synthetic aperture radar (SAR), enables radar to produce high resolution images in both range and azimuth directions.

The work presented in this thesis uses SAR for oil well monitoring. SAR is seen as a good candidate to follow oil well changes in time by means of maintenance. Other methods to perform this task have been introduced and implemented but they are not able to produce high resolution images from the oil well. Using SAR for oil well monitoring provides high resolution images of oil well walls in order to detect the asphaltene or bitumen. The resolutions of images can be enhanced by using UWB signal and SAR processing. Asphaltene and bitumen are the heavy components of crude oil and capable of blocking the porous media in oil well. The porous media is called damaged material when its holes are blocked by asphaltene or bitumen as it cannot pass the oil any more. A decrease in oil production is the consequence of this phenomenon. If these materials can be detected at very beginning stages of formation, addition of solvent at the location of the detected materials can be very helpful for oil well maintenance.

This thesis is divided in to two parts. The first part focuses on SAR processing whereas the second one aims at antenna design and fabrication to work in a ground penetrating synthetic aperture radar (GPSAR) system. In the first part, an oil well model based on the measured electrical properties of common oil well materials is introduced. SAR processing is then applied to the oil well model to reconstruct SAR image of the oil well. The resulting SAR image is shown to provide high resolutions so that different materials can be distinguished. In the second part, a modified TEM horn antenna for SAR is designed, simulated and fabricated. The antenna is customized to work in oil media. A new profile model for the TEM horn antenna is proposed that modifies the antenna radiation pattern in the design. The antenna measurements are shown to be in agreement with the simulated results.

Contents

Figures list

PREFACE

This master thesis summarizes my work in field of oil well monitoring with synthetic aperture radar. This work has been performed at Department of Electrical Engineering at University of Alberta where I was working on my thesis as a visiting student.

This thesis consists of two introduction chapters to the field of SAR processing and TEM horn antenna design followed by two scientific papers:

- *D. Oloumi, P. Mousavi, M.I.Pettersson, D. Elliott, "Detection of Near-Wellbore Formation Damage using Synthetic Aperture Radar", IEEE Transactions on Geoscience and Remote Sensing, submitted for publication.*

- *D. Oloumi, P. Mousavi, M.I.Pettersson, D. Elliott, "A Modified TEM Horn Antenna Customized for Oil Well Monitoring Applications", IEEE Transactions on Antenna and Propagation, submitted for publication.*

Acknowledgements

It would not have been possible to write this Master thesis without the help and support of the kind people around me. It is possible to give particular thanks to some of them here.

Above all, I would like to thank my wife, Atefeh, for her great support and patience especially during the time I was working on my thesis. I would like to give my sincere thanks to my parents Maryam and AMIR and my siblings (Elahe and Benjamin) who have always been supporting me in all parts of my life for which my mere expression of thanks likewise does not suffice.

I would like to thank my supervisor Prof. Mats Pettersson at Blekinge Institute of Technology for his guides and helps and my supervisors Dr. Pedram Mousavi and Prof. Duncan Elliott at University of Alberta for accepting me as a visiting student and providing me with good advises during this thesis.

I would like to thanks Dr. Viet Tu Vi and Mr. Thomas Sjörgen for their help to teach me SAR processing concepts during this project.

I would like to thank Shlumburger DBR center and Dr. Kamran Akbarzadeh for giving me the opportunity to work on this project.

I also would like to thank my bachelor's thesis supervisor, Prof. Farrokh Hojjat kashani who directed me to this field of study by his deep knowledge and attitudes.

Thanks to Natural Sciences and Engineering Research Council of Canada (NSERC) for funding this project.

At the end, I would like to thank my indeed friends who have always been supporting me in need.

Background and Motivation

Oil benefits our living and society in many ways and today is one of the most important natural resources in the world. From its applications in plastic industry used in e.g. packaging, tires, cars, houses and instruments to its key function as fuel in transportation and industry sector as oil is still the main source of power in many fields. Oil well maintenance is one of the most important issues in oil and gas industry nowadays. Maintaining an existing oil well is cheaper than installing another well.

Formation damage is an undesirable operational caused by asphaltene deposition inside porous media. Oil, gas, water and etc. come out through porous media to the oil well hence any impairment with porous media consequences to reduction in oil production. This phenomenon can occur during the various phases of oil and gas recovery from subsurface reservoirs. Formation damages are indicated by different signs like well permeability impairment, skin damage, and reduction of well performance. As formation damage is not a reversible procedure, porous media should be monitored to maintain the well instead of constructing another well to reduce cost.

Asphaltene deposition causes the most common organic near-wellbore formation damage. Pieces of Asphaltene are shown in Fig. 1.1. The consequences of asphaltene impairment are the reduction of the oil productivity of reservoir that may causes a noneconomic operation. Accordingly, it is essential to evaluate the reservoir rock and determine its characteristics and the level of damage. Currently methods like X-ray scanning, nuclear magnetic resonance (NMR) scanning, magnetic resonance imaging (MRI), and acoustic tomography techniques are being used to evaluate the damage evaluation of the extracted samples from oil well.

This thesis uses ground penetrating radar (GPR) to imaging the oil well surrounding and tries to simulate a novel microwave imaging technique for oil well. The proposed method is the combination of GPR technique for obtaining necessary penetration depth and the required range resolution; and synthetic aperture radar (SAR) to obtain the more lateral resolution to build up a ground penetrating synthetic aperture radar (GPSAR). This combined technique gives better image resolution. Fig. 1.2 shows the proposed configuration for oil well monitoring. The objective of this thesis is to investigate and find the design parameters to simulate the proposed

method. This thesis work is mainly presented in two papers (Part I and Part II). In this introduction these two areas of SAR processing and TEM horn antenna design are introduced.

Fig. 1.1 . Asphaltene

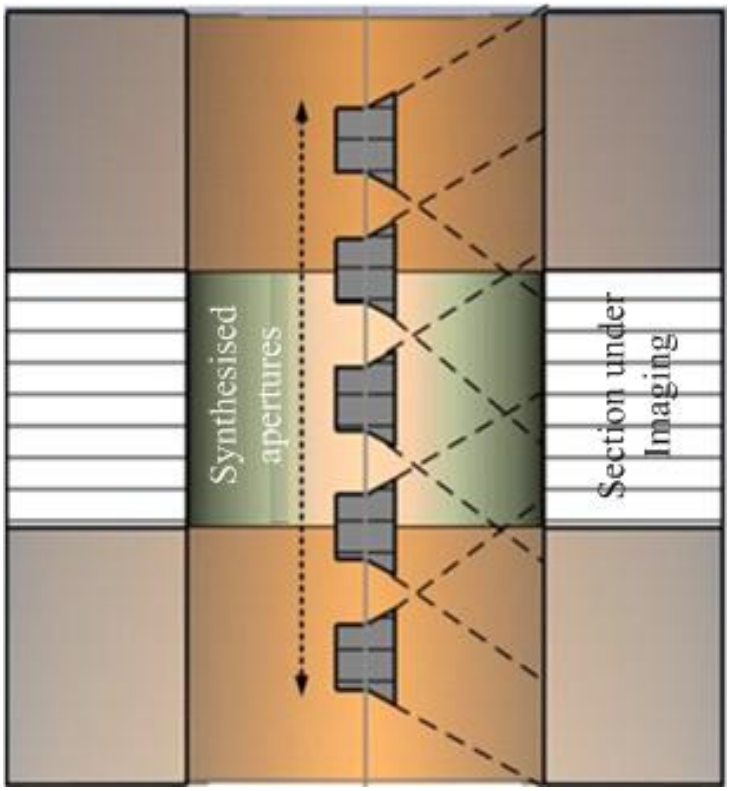

Fig. 1.2 .Ground penetrating synthetic aperture radar for oil well monitoring.

Synthetic Aperture Radar Processing

As synthetic aperture radar (SAR) processing is used in this work, the theoretical background of SAR will be presented here. In SAR processing, the aperture is synthesized by processing the pulses received at the aperture positions. The pulses are collected when the real antenna is moving over an area of interest. The purpose of processing these pulses is to create high resolution SAR images.

2.1 CHIRP SIGNAL

"Chirp signal" is widely used in SAR due to its good correlation property [1-7]. This property increases the pulse resolution using the match filtering technique. A chirp signal is generated by a linear sweep over frequency. It is therefore called linear frequency modulated (LFM) signal. For a chirp signal, the signal frequency can increase from low to high and vice versa, decrease from high to low. A chirp signal has constant amplitude, pulse width T_p, center frequency f_c, and a phase component $\phi(\tau)$ that varies with time. The complex representation of a chirp signal is given by [6, 7]

$$s(\tau) = \text{rect}\left(\frac{\tau}{T_p}\right) \exp\{\text{j}2\pi f_c \tau + \text{j}\pi K \tau^2\} \quad (1)$$

Where K is the LFM rate or chirp rate, τ is the time variable and "rect" refers to a rectangular function of time τ and pulse duration T_p. Fig. 2.1.a plots the real and imaginary parts of a chirp signal with frequency range from 1.4 to 11 GHz. As shown, the real and imaginary parts are oscillating. The phase of the signal is expressed by [6, 7]:

$$\phi(\tau) = \pi K \tau^2 \quad (2)$$

By taking the first derivation of phase $\phi(\tau)$, instantaneous frequency can be calculated as [6, 7]:

$$f = \frac{1}{2\pi}\frac{d\phi(\tau)}{d\tau} = K\tau \quad (3)$$

Equation (3) shows that the frequency is a linear function of time and the slop of the function depends on the value of K.

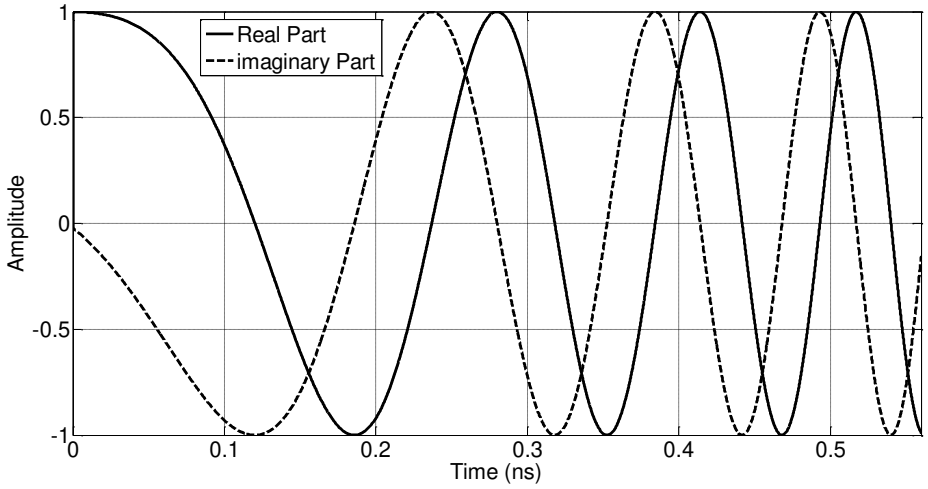

(a)

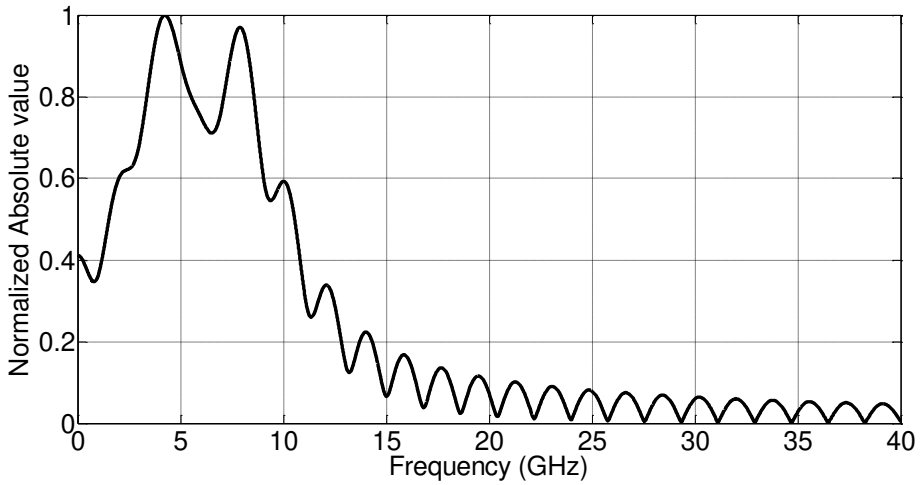

(b)

Fig. 2.1. (a) Chirp Signal (b) Corresponding frequency spectrum.

.

Bandwidth (BW) is the range of the swept frequencies from low to high or vice versa. It is defined by the product of the absolute value of the chirp rate and the pulse width. The positive or negative values of K results in the up chirp or down chirp, respectively. The pulse width T_p or in other words the sweep time is a very important factor since it determines the detection range which will be explained later. The signal showed in Fig. 2.1.a is an up chirp pulse.

$$BW = |K|\, T_p \tag{4}$$

2.2 SPECTRUM OF CHIRP SIGNAL

The chirp signal spectrum is obtained by taking Fourier transform of the chirp signal. Equation (5) shows the mathematical expression of linear chirp signal Fourier transforms.

$$S(f) = \int_{-\infty}^{\infty} \text{rect}\left(\frac{\tau}{T_p}\right) \exp\{\text{j}2\pi f_c \tau + \text{j}\pi K \tau^2\}.\exp\{-\text{j}2\pi f\tau\}\, d\tau \quad (5)$$

This transform is done using discrete Fourier transform (DFT). Fig. 2.1.b shows the spectrum in frequency domain (from 0 to 40 GHz) of the transmitted signal given in Fig. 2.1.a. As seen, most of the signal energy is carried by frequency components in the range from 1.4 to 11 GHz.

2.3 PULSE COMPRESSION AND MATCHED FILTERING

To achieve a high pulse resolution, a signal with very narrow mainlobe is needed. Such signal is employed to measure distance, reflectivity, shape and speed of objects. Pulse compression is a signal processing technique to increase SNR and to secure good resolution in range direction and introduced as a solution to improve range resolution [3-5].

Pulse compression is based on the auto correlation function of transmitted signal which is known as match filtering. This method is called "pulse compression" as well. By applying pulse compression, the energy of the signal with the pulse duration of T_p is compressed to a signal having narrow mainlobe and approximated to a Sinc function which contains more than 90% of total energy. The operation is done by a convolution between received and transmitted signals. The convolution output is given by [3]:

$$s_{out}(\tau) = (T_p - |\tau|)\text{rect}\left(\frac{\tau}{2T_p}\right)\text{sinc}[\kappa\tau(T_p - |\tau|)] \quad (6)$$

It shows that most of signal energy is accumulated in the Sinc mainlobe which results in high power concentration and fine resolution pulse with the same energy of the sent chirp signal. The received chirp pulse and its matched pulse are shown in Fig. 2.2. As can be seen the signal is not smooth. This problem can be solved by interpolating the recived signal beffore match filtering.

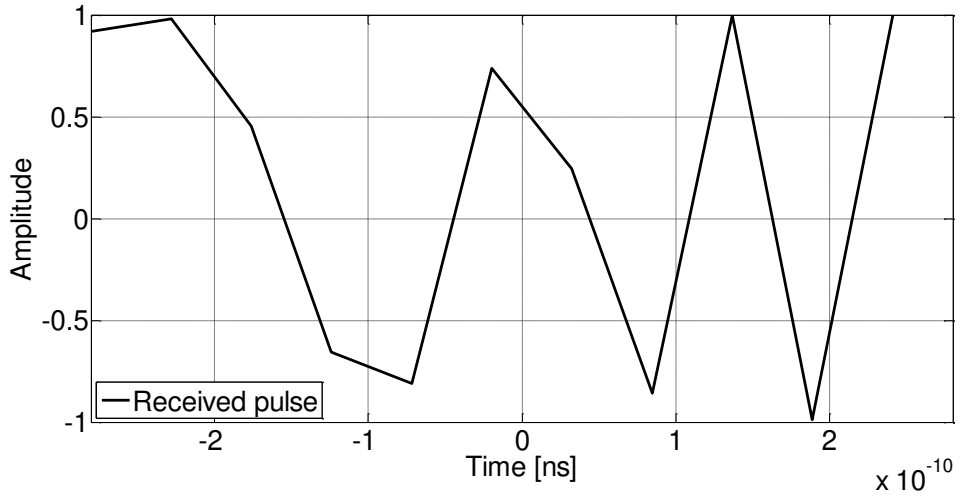

(a)

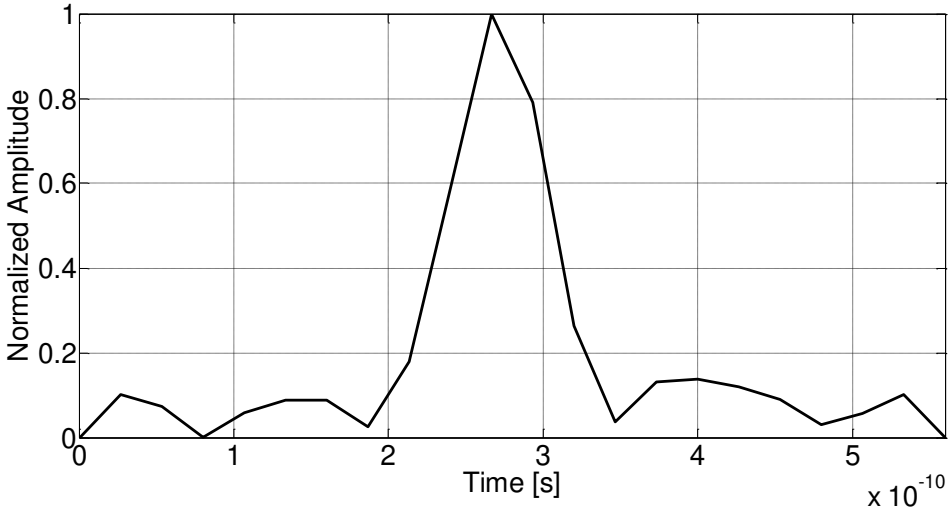

(b)

Fig. 2.2. (a) Chirp pulse before interpolation (b) corresponding match filter out put

2.4 INTERPOLATION

The received signals at receivers are sampled with the Nyquist sampling rate which is twice of the signal bandwidth. From samples of the discrete signal, other samples of the signal can be reconstructed by interpolation techniques [8]. In SAR processing, a signal sample is selected according to the delay time. Interpolation is necessary to increase accuracy of finding the sample associated with the time delay. In other word, raw data should be oversampled in order to

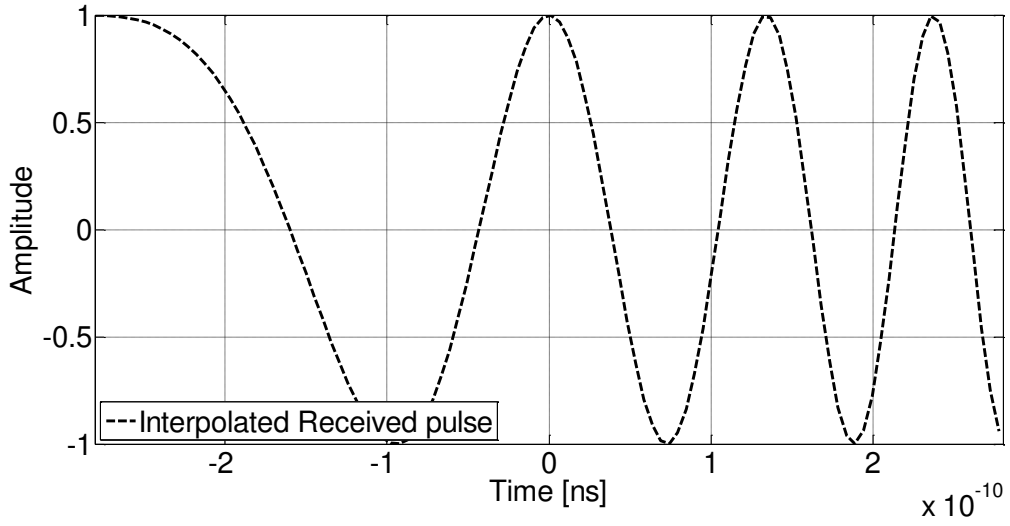

(a)

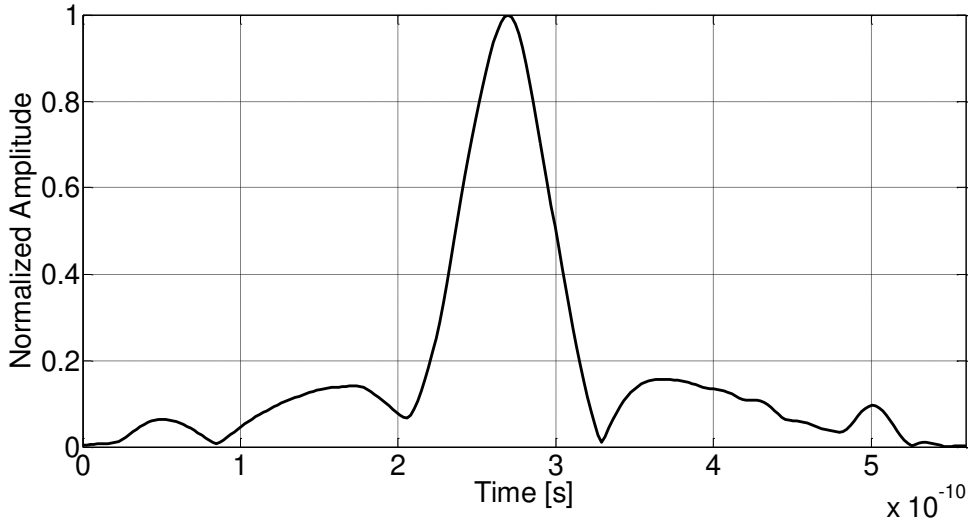

(b)

Fig. 2.3. Interpolated Chirp pulse (b) corresponding match filter out put

decrease interpolation errors.

In this thesis, interpolation is used to enhance SAR image quality. There are many available interpolation methods and the easiest one is to use the nearest neighbor method. However, the approximation of the method is not always the best choice. Other interpolation methods which have been used for image quality improvement are linear, quadratic and Sinc interpolation [8]. Fig. 2.3.a depicts the interpolated version of received signal shown in Fig. 2.2.a. As can be seen chirp pulse after interpolation is fairly smooth so the match filter output is also smoother in

comparison with not interpolated one (Fig. 2.2.b). The interpolation is carried out by "spline" function which is one of the functions in Matlab interpolation techniques. The oversampling rate is 10. As can be seen from Fig. 2.3 samples between the existing samples are generated by interpolation and which makes the received signal smoother.

2.5 GLOBAL BACKPROJECTION

Global Backprojection (GBP) algorithm is the first time-domain algorithm for SAR image reconstruction [9-10]. Other time-domain algorithms have been developed on GBP's basis. GBP has both advantages and disadvantages. The main advantage of GBP is that there is no limitation on the image size. Besides this, GBP can handle extreme range migration and large motion compensation. However, the high computational load, which depends on numbers of aperture positions and image samples, is the only drawback of this algorithm. The smaller image sample results in higher image quality but requires more computations. Hence, the high computational load is the price to pay for such unique features of GBP.

2.5.1 SAR RAW DATA ACQUISITION

In this section, we represent the produce to acquire the raw data for SAR processing. The SAR scene is simulated by a point-like scatterer located at the center of the SAR scene. The dimension of the SAR scene is defined by 2.5 meter aperture length and 0.5 meter depth. The coordinates of the scatterer is x0=2.5 and z0=0.25 as shown in

Fig. 2.4. The black dots in

Fig. 2.4 show the aperture positions or in other words the positions of the antenna which sends the chirp signal and receive the reflections. The set of the reflections collected at all aperture positions are called the raw SAR data as they are not processed. The raw data is in spatial domain in one direction (azimuth) and in time domain in another (range). Since the antenna moves over the aperture, the distance between the antenna and the scatterer will change. The different distances between aperture positions and scatterer make different time delays for SAR processing.

After pulse compression, the image scene of the data appears as a hyperbolic curve (hyperbola) as shown in Fig. 2.5.

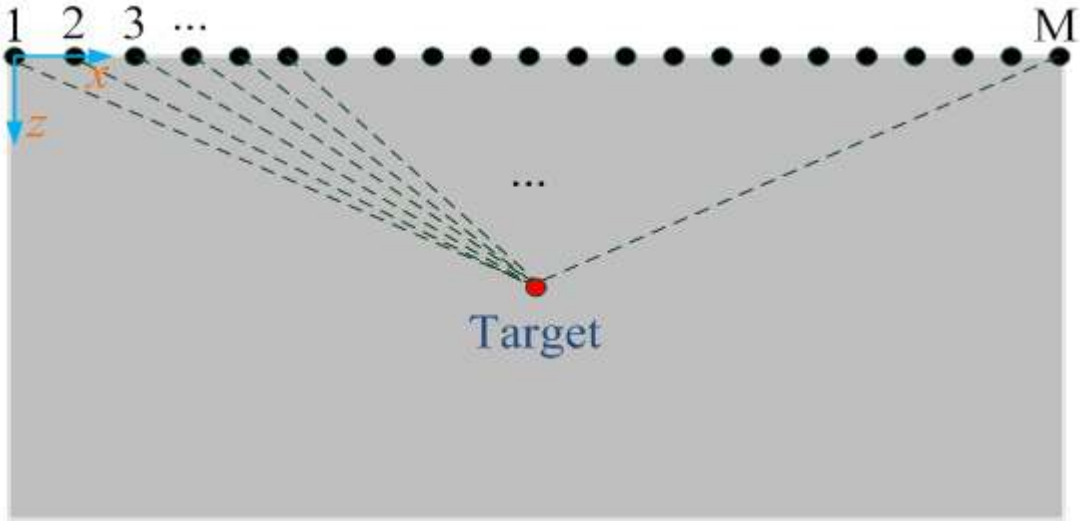

Fig. 2.4. Point target

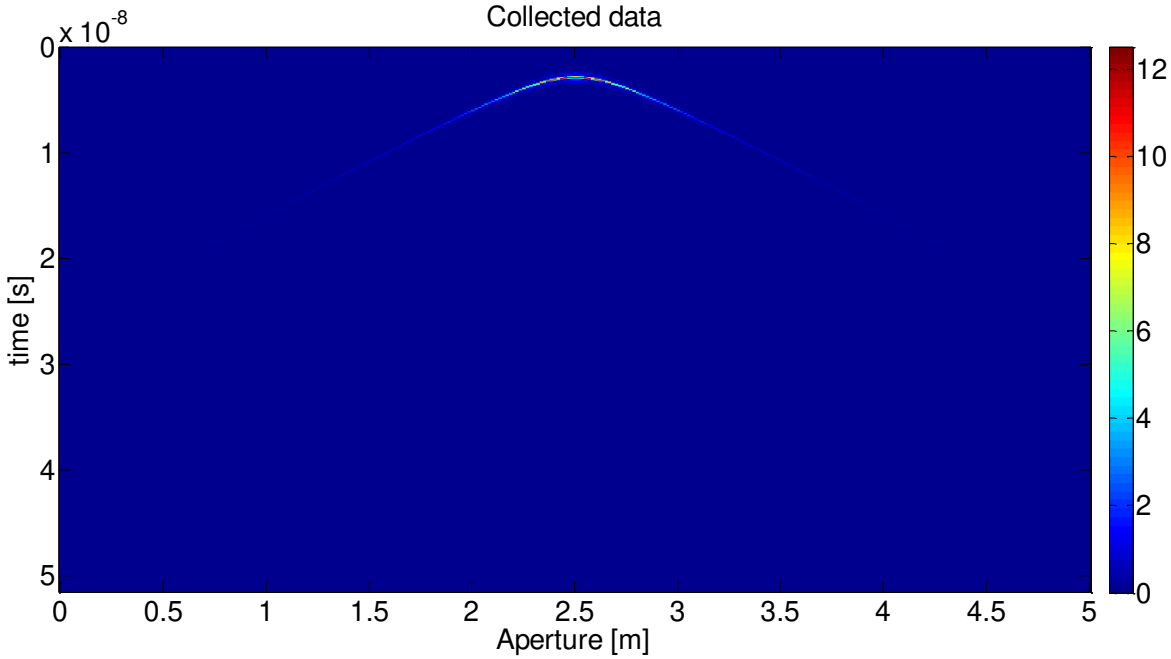

Fig. 2.5. SAR Raw Data

The interpolation can also be applied to increase the number of the data samples. GBP is then used to concentrate the energy of the hyperbola to a single point (at the center of hyperbola).

2.5.2 SAR DATA PROCESSING BY GBP

GBP is capable of forming high quality SAR images. A SAR image is constructed in one step and there are no intermediate steps like beam-forming in between. The superposition of radar echoes with respect to the time-dependent ranges to reconstruct an image sample (x, z) is interpreted by the integral [9-10].

$$h(x,z) = \int_{-\frac{L}{2}}^{+\frac{L}{2}} g(x, Rp)\, dx \tag{7}$$

The range "Rp" between an aperture position (x_{pf}, z_{pf}) and the sample (x, z) as shown in Fig. 2.5, is represented by the hyperbolic function.

$$R\mathrm{p} = \sqrt{\left(x_{pf} - x\right)^2 - (z_{pf} - z)^2} \tag{8}$$

The SAR image reconstruction is carried out in the following steps. First, an empty SAR image $M \times N$ grid in the image plane is defined. Secondly, the range Rp between an aperture position and the image pixel is calculated. Based on Rp, we can estimate the delay time by $\mathrm{t_d} = 2Rp \,/\, \mathrm{c}$ (where c is the speed of propagation in the medium) and the vector index corresponding to the estimated delay time. The index is calculated by dividing the calculated time delay by sampling time. Finally, the radar signal sample associated with the calculated index is assigned to that image sample. The procedure is repeated for all aperture positions as expressed by Equation (7, 8). As match filtering is employed for pulse compression, the time delay due to match filtering, which is half of pulse width, should be considered in the time calculation as well.

An algorithm to implement Matlab code is given as follow:

Do loop on l = 1 to Number of apertures

Do loop on m = 1 to Number of samples in X- direction

Do loop on n = 1 to Number of samples in Z- direction

R (l, m, n) = Calculate the distance between aperture position l and image sample (m,n)

Time (l, m, n) = Calculate the corresponding flight time to each pixel from different aperture positions

Finding the corresponding index by dividing the flight time by sampling time (time resolution)

Putting the found value from signal to the pixel

Finish loop

Finish loop

Sum the assigned value to the pixel from different position

Finish loop

The SAR image reconstructed from non-interpolated raw data with GBP is shown in Fig. 2.6. SAR image includes one single point-like scatterer in the middle of the SAR scene as it was defined already. As can be seen there are some background noise especially around the scaterer in the SAR image. This background noise is due to the interpolation error. This error is because of selecting wrong sample as the number of samples in time is not enough. To reduce this error raw data should be interpolated before SAR processing.

The background noise around the target can be reduced by using an appropriate interpolation. The interpolation can be done by any rate. The higher rate gives more samples of the data. The interpolation is based on the “spline” interpolation which is available in Matlab with the over sampling rate of 10. As can be seen, SAR image in Fig. 2.7, the background noise level is reduced significantly and the scaterer is more obvious now. Small figures in corners show the close shut of the target. It can be understood mistakenly that the resolution in range direction is decreased after interpolation. But this is not correct. The image constructed without interpolation raw data (Fig. 2.6) does not have enough samples for different time to assign to different pixels.

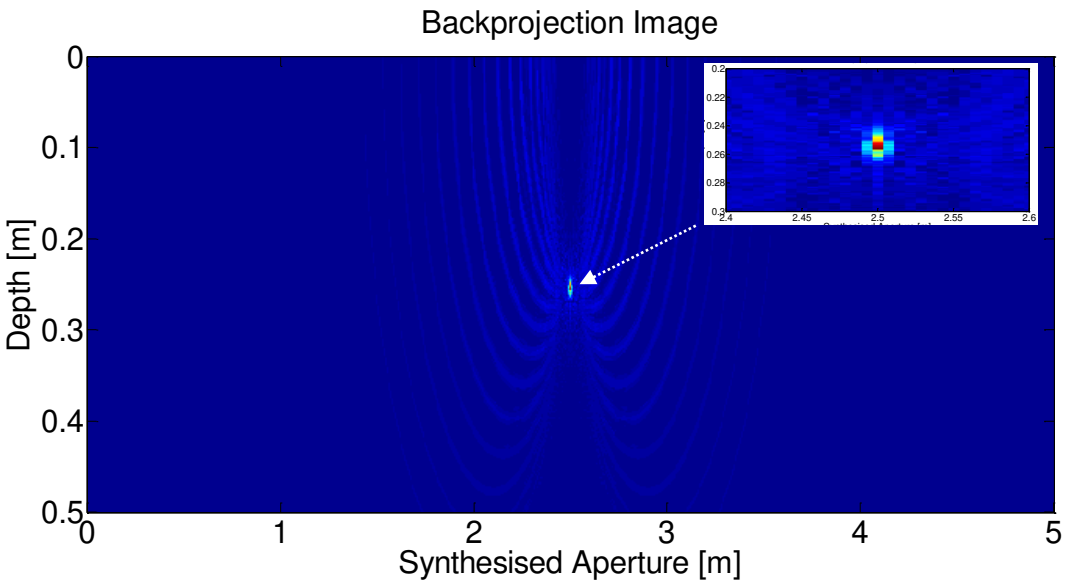

Fig. 2.6. SAR Image of the Point Target by GBP Algorithm

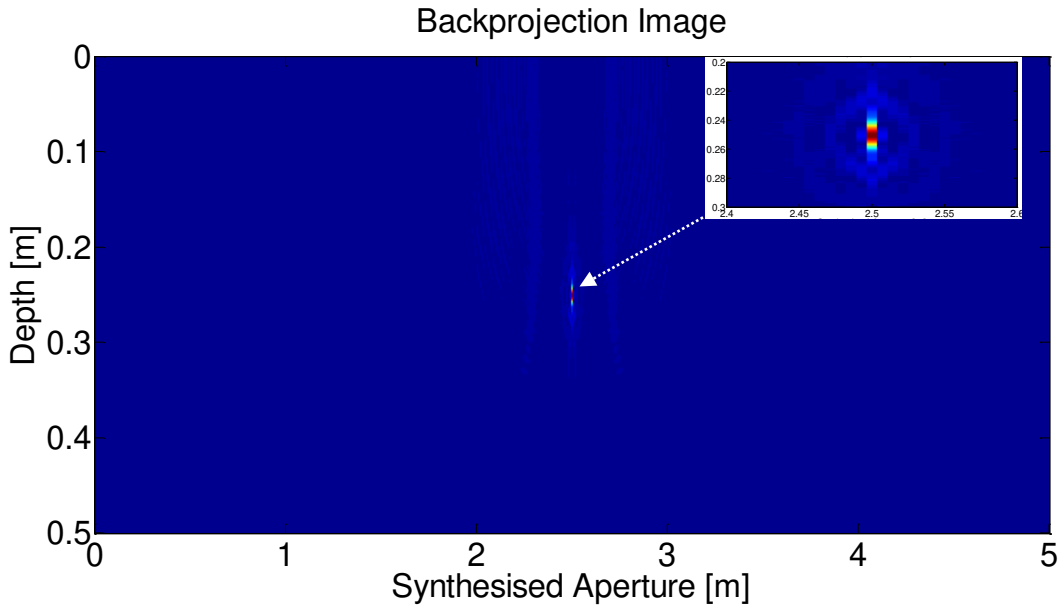

Fig. 2.7. Interpolated SAR Image of the Point Target by GBP Algorithm

So wrong values are gotten that makes the background noise as well. After interpolation as the number of samples is increased in time so the time samples are selected by more accuracy. The length of both Sincs (interpolated and not interpolated) is the same but the interpolated imaged illustrates smother Sinc in range direction while this is not happened for not interpolated image.

TEM Horn Antenna

In this thesis a modified TEM horn antenna design, simulation and fabrication is presented for oil well monitoring applications. This section is an introduction to explain about conventional TEM horn antenna design like impedance matching, feeding system and some antenna characteristic definitions like mainlobe, side lobe and etc. will also be explained.

3.1 ANTENNA CHARACTERISTIC DEFINITION

Antenna radiation pattern is the strength of radiated radio power in each angle with in a sphere. The radiated power by considering antenna loos is called antenna gain in specific direction as well. Different antenna has different radiation pattern that is very much dependent on antenna shape by generating current distribution over the antenna surface. Hence, antenna radiation pattern can be controlled by altering current distribution.

Antenna radiation pattern can be introduced by mainlobe, sidelobe, and backlobe. The main portion of energy is radiated through the antenna mainlobe. That is why it is called antenna mainlobe. Other unwanted lobes around mainlobe are called sidelobe as they are radiating power in other directions. The sidelobe in opposite direction of mainlobe is called backlobe and the ratio of power radiated from front (mainlobe) and back (back lobe) is the antenna front to back ratio (F/B). In most cases the more F/B is the better but it differs for different applications. An antenna radiation pattern is depicted in Fig. 3.1. All main, side and backlobes are shown here. Horizontal axis is in degree while vertical axis is antenna gain. Antenna theory book written by CONSTANTINE A. BALANIS [11] is one of the best references to have more studying about these definitions.

3.2 TEM HORN ANTENNA

Ultra wide-band (UWB) antennas are demanding for many ultra-wideband applications like UWB pulse radar and broad band communication systems. Different kinds of UWB antennas like bow-tie, log periodic dipole array antenna, spiral, and ridge horn antenna have been working in mentioned applications [12-15].

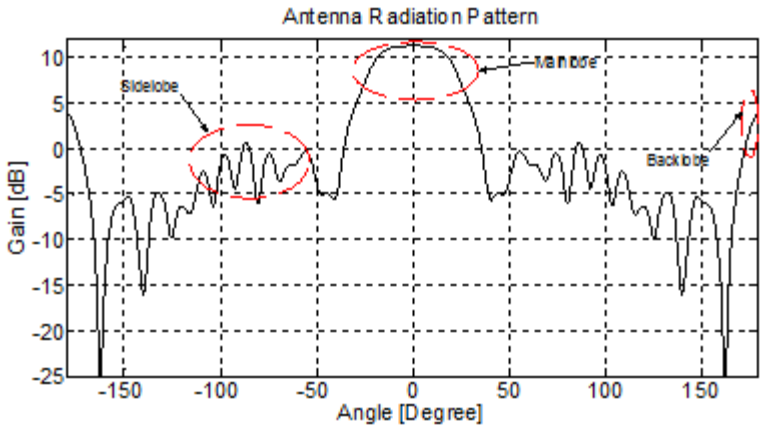

Fig. 3.1.Antenna Radiation pattern

TEM horn antenna is one of most well-known UWB antenna that has been used in many ground penetrating radar system due to its UWB characteristics [16-17].

TEM horn antenna is made by two tapered metal plates. This structure guide current flows on antenna flares to generate TEM wave propagation. Magnetic and electric fields are generated by flowing currents and voltage difference between and over the plates accordingly. A TEM horn antenna is a kind of impedance transformer from transmission line to the medium of propagation. Different plate widths along with different gap between antenna plates produce variations of impedance that has to be calculated carefully to minimize reflection coefficient for ultra-wideband of frequencies. Next section is dedicated to explain the conventional TEM horn antenna design in detail.

3.3 CONVENTIONAL TEM HORN ANTENNA DESIGN

Antenna size is related to the operation frequency. Wavelength is the distance that the radio wave travels during one cycle and is given by dividing the light velocity by the operation frequency. Therefore, the higher operating frequency results in smaller antenna size. Antennas can be categorized by their length such as half or quarter-wavelength dipoles. The length of antenna determines its resonant frequency as antenna has the best matching for radiation around this frequency. Hence, different antenna length is associated to different kinds of antenna. TEM horn Antenna length is considered to be about half wave length approximately at the lowest

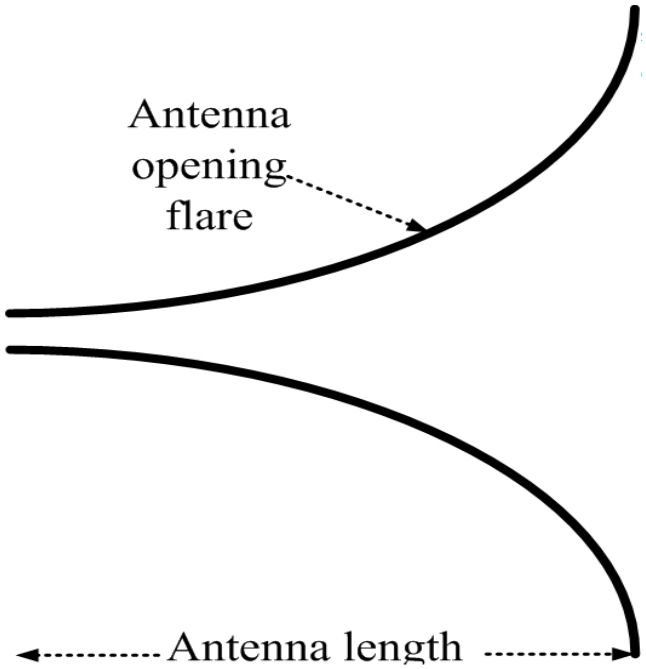

Fig. 3.2. Conventional TEM horn antenna side view.

frequency [16]. This length gives the antenna cut of frequency (lower frequency) while upper frequencies can be achieved by impedance matching. As it is mentioned TEM horn antenna is an impedance transformer to transfer feed impedance to the medium of propagation impedance. This impedance transformation can be done by different profile. One of the best profiles for impedance matching is exponential curve. Antenna profile grown by exponential curve is shown in Fig. 3.2 and called antenna flare or opening flare. The opening flare is divided by the number of sections (N) for impedance calculation. For exponentially tapered transformation the impedance of each section is expressed as:

$$\mathrm{Z}(z_i) = \mathrm{Z}_0\, e^{\alpha.d_i} \tag{1}$$

In which the *di* is the section length and is given by:

$$d_i = \frac{\mathrm{iL}}{\mathrm{N}} \text{ for } \qquad \mathrm{i} = 1, 2, 3, \ldots, \mathrm{N} \tag{2}$$

$$\alpha = \frac{1}{L}\ln(\frac{\eta}{Z_0}) \tag{3}$$

Z_0 is considered to be 50 Ω as the feed line impedance, η is the intrinsic impedance of the medium of propagation which is $(\frac{120\,\pi}{\sqrt{\varepsilon_r}})$ Ω, L is the total antenna length; N is the number of the sections and α is the expansion constant. Antenna plates separate from each other by an exponential function [19].

$$Gap(\mathrm{di}) = \mathrm{a}.\,\mathrm{e}^{\mathrm{b.d_i}} \tag{4}$$

In which, "*a*" and "*b*" are constants which are determined by:

$$a = Gap_{first} \;\;\&\;\; b = \frac{1}{L}\left(\frac{Gap_{end}}{Gap_{first}}\right) \tag{5}$$

"Gap $_{first}$" and *"Gap $_{end}$"* are the smallest and longest separation between parallel plates at start and end point of aperture respectively. To determine the plate width of each section, *W (zi)*, the characteristic impedance of a parallel plate waveguide *Z (z_i)*, given by [24], is used:

$$\mathrm{Z}(z_i) = \left(\frac{Gap(d_i)}{W(d_i)}\right) \tag{6}$$

The explained parameters are demonstrated in Fig. 3.3.

3.4 ANTENNA FEEDING SYSTEM

Balun is a transformer that converts unbalance to balance line or balance to unbalance. The word of ***Balun*** is taken from the first letters of ***bal***ance to ***un***balance. When an antenna with symmetric structure is going to be fed by a coaxial line which is not balance line, it causes un-symmetrically in radiation patterns. This problem is due to difference between currents over coax shield and inner conductor.

TEM horn antenna is a balance structure as it is kind of dipole so a balun is needed to excite this structure. Different kinds of balun structure are employed to feed different type of TEM horn antenna [18-22]. In this thesis we are using U-shape cavity balun for its very good wideband characteristics [18-19]

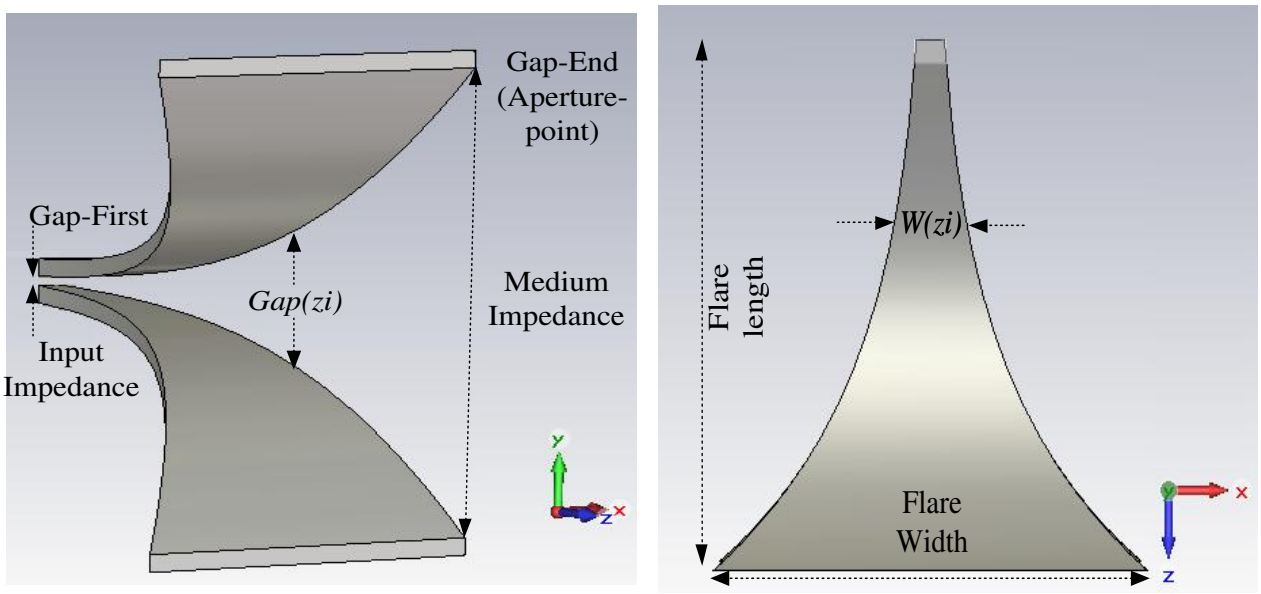

(a) (b)

Fig. 3.3. (a) Conventional TEM horn Antenna structure view (a) perspective (b) top.

3.5 REFERENCES

[1] J. C. Curlander, and R. N. McDonough, "Synthetic Aperture Radar: Systems and Signal Processing," Hoboken, New Jersey, John Wiley & Sons, 1991.

[2] N. Levanon and E. Mozeson, "Radar Signals," 1st edition, Hoboken, New Jersey, Wiley-IEEE Press, 2004.

[3] A.G .Stove, "Linear FMCW radar techniques," Radar and signal processing, IEEE Proceeding F. Vol. 139, No.5, pp.343–350, 1992.

[4] I. Ahmed, "Study of the Local Backprojection Algorithm for Image Formation in Ultra Wideband Synthetic Aperture Radar," M.S. thesis, Signal processing. Dept., Blekinge Institute of Technology. Karlskrona, Blekinge. 2008.

[5] A. J. Zejak, I. S. Simic, B. M. Zrnic , "Chirp radar ambiguity function shaping," EUROCON 2001, International Conference on trends in Communications, Belgrade, 2001, Vol.2, pp.325-328.

[6] I. G. Cumming, and Wong F. H, "Digital Processing of Synthetic Aperture Radar Data; Algorithms and Implementation," Artech House, 1st edition. Norwood, MA, USA, 2005.

[7] M. Soumekh, "Synthetic Aperture Radar Signal Processing with Matlab Algorithms," John Wiley & Sons, Inc., 1999.

[8] Alan V. Oppenheim, Ronald W. Schafer, "Discrete-Time Signal Processing," 3rd Edition, Prentice Hall Signal Processing, 2009.

[9] V. T. Vu, T. K. Sjögren, M. I. Pettersson, and A. Gustavsson, "Definition on SAR image quality measurements for UWB SAR," In proc. *SPIE Image and Signal Processing for Remote Sensing XIV*, Vol. 71091, Cardiff, UK, Sep. 2008, pp.79091A (1-9).

[10] L. E. Andresson, " On the determination of function from spherical averages," SIMA Journal on Mathematical Analysis, Vol. 19, no. 1, pp. 214-232, 1988.

[11] Constantine A. Balanis, "Antenna Theory: Analysis and Design," 3rd Edition, John Wiley & Sons, Inc., 2005.

[12] D. A. Kolokotronis, Y. Huang, and J. T. Zhang, "Design of TEM horn antennas for impulse radar," IEEE High Frequency postgraduate student colloquium, Leeds, pp. 120–126, 1999.

[13] R. T. Johnk, D.R. Novotny, C.M. Weil, M. Taylor, and T. J. Hara, "Efficient and accurate testing of an EMC compliance chamber using an ultra-wideband measurement system," IEEE International Symposium on EMC, Montreal, 2001, Vol. 1, pp. 302–307.

[14] J. H. Kim, and J. I. Park, "TEM horn antenna for the time domain shielding effectiveness measurement," IEEE International Symposium on EMC, Beijing, 1997. pp. 265–269.

[15] C. Nguyen, J. S. Lee, and J. S. Park, "Ultra wideband microstrip quasi-horn antenna," IEE Electronics Letters, Vol. 37, pp. 731–732, 2001.

[16] A. S. Turk, "Ultra wideband TEM horn design for ground penetrating impulse radar system," Microwave and Optical Technology Letters, Vol. 41, No. 5, pp. 333–336, 2004.

[17] G. Y. Chen, J. S. Sun, S. Y. Huang, and C. J. Huang, "The tapered TEM horn antenna design for EMC and radiation measurement," 7th International Symposium on Antennas, Propagation & EM Theory, Guilin, 2006, pp. 1-4.

[18] A. R. Mallahzadeh and F. Karshenas," Modified TEM horn antenna for broadband applications," Progress In Electromagnetics Research, Vol. 90, PP. 105-119, 2009.

[19] L.L. Chen, C. Liao, Lei Chang, Xuan Zheng, Gang Su, Jian Fang ,"A novel ultra-wideband knife-shape TEM horn antenna design for transient application," International Conference on Microwave and Millimeter Wave Technology (ICMMT), Chengdu, 2010, pp.355-358.

[20] J. W. Duncan and V. P. Minerva, "100:1 bandwidth balun transformer," Proceedings of the IRE, Vol. 48, No. 2, pp. 156-164, 1960.

[21] P. R. Foster, S. M. Tun , " A wideband balun from coaxial line to TEM line," Ninth International Conference on Antennas and Propagation, Eindhoven, vol.1, pp. 286 – 290, 1995.

[22] K. Chung, S. Pyun, and J.Choi, "Design of an Ultrawide-Band TEM Horn Antenna with a Microstrip-Type Balun," IEEE Trans. Antennas Propagation, Vol. 53, No. 10, October. 2005.

Part I

"Detection of Near-Wellbore Formation Damage using Synthetic Aperture Radar"

Part I:

D. Oloumi, P. Mousavi, M.I.Pettersson, D. Elliott, "Detection of Near-Wellbore Formation Damage using Synthetic Aperture Radar," IEEE Transactions on Geoscience and Remote Sensing, submitted for publication.

Detection of Near-Wellbore Formation Damage using Synthetic Aperture Radar

4.1 ABSTRACT

A borehole imaging method for nonconductive medium using UWB synthetic aperture radar is studied in this paper. This approach provides higher quality images and more advantages in comparison with conventional dielectric or resistivity imaging tools. A high resolution image in both down-range and cross-range is obtained by using an ultra-wide band electromagnetic (UWB EM) pulse from 1.4 GHz to 11 GHz and synthesizing the apertures in down-range and cross-range respectively. A simulation of an oil well with concrete wall is done based on measured dielectric properties data of oil well materials. We simulate a proposed down-hole measurement intended to detect formation damage caused by asphaltenes blocking oil flow through porous media within 0.5 m of the well bore. Simulation results show that the damaged material which is a challenging problem in oil industry is detected and localized through this method. An ultra-wideband antenna is also designed as a transceiver for this radar system.

4.2 INTRODUCTION

Reservoir management employing remote sensing is emerged as a new important concept in the oil and gas field. In particular, having sensors capable of tracking the dynamic behavior of reservoir in the proximity of production wells would provide geologist, geophysicists and petrophysicist with valuable information about formation evolution to reservoir management.

Formation damage inside oil wells is a generic terminology referring to the impairment of the permeability of petroleum- bearing formation by various adverse processes. Formation damage assessment, control, and remediation are among the most important issues to be resolved for efficient exploitation of hydrocarbon reservoirs [1]. Formation damage may be caused by many factors, including physico-chemical, chemical, biological, hydrodynamic, and thermal interactions of porous formation, particles, and fluids, and the mechanical deformation of formation under fluid shear stress. Formation damage indicators include permeability impairment, skin damage, and decrease of well performance. As stated by Porter [2], “Formation

damage is not necessarily reversible" and "What gets into porous media does not necessarily come out." Therefore, it is better to avoid formation damage than to try to restore it. The most often occurring organic near-wellbore formation damage is due to asphaltene or bitumen deposition. The formation damage due to asphaltene occurs in shallower depth [3]. The consequences of asphaltene impairment are the reduction of the oil productivity of reservoirs and uneconomical operation. Therefore, it is essential to evaluate the reservoir rock to determine its characteristics and the level of damage.

Currently methods like X-ray scanning, nuclear magnetic resonance (NMR), magnetic resonance imaging (MRI), and acoustic tomography techniques are being used to damage evaluation of extracted samples. However, reservoir rock evaluation is a very expensive and cumbersome task requiring preserved rock samples from the production zone, a multidisciplinary effort with knowledge of instrumentation, data acquisition, testing and interpretation, and analysis and cross-correlation of various types of data [4]. Conventional micro-resistive and ultrasonic borehole imaging technology was popular for nonconductive mud systems in 1990s [3& 5]. Oil-based mud systems in most cases are not capable of providing high-resolution images.

Borehole radar is introduced as a promising sensor inside oil well to monitor the reservoirs [6]. Many borehole radars are introduced to collect well-bore information in an azimuthal range of 360 degree of surface or any target detection [7-11]. A theory modeling of the dielectric logging tool at high frequencies is discussed by Chew [12]. Damage materials get new dielectric properties that discriminates them from other materials. The detection and distinction between different materials in a medium can be done by their reflection to an EM wave. A high-frequency electromagnetic (EM) short pulse was introduced to make image for nonconductive fluid [13]. Using EM short pulse shows more advantages in comparison with conventional dielectric or resistivity imaging tools with respect to image quality.

The pervious proposed methods cannot distinguish between the materials in oil well as it needs high resolution radar in both down and cross range. That is because of the low dielectric contrast between oil-sand and asphaltene as it is measured and demonstrated in this paper. Very narrow pulse width and also highly directive antenna are the solution to the range and the cross range resolution accordingly.

The problem with highly directivity antenna is its size which cannot be accommodated in the oil well. Here, we use the benefits of synthetic aperture radar (SAR) processing by coherent summation of received pulses instead of using highly directive antenna to collect the energy of each point to the right place.

In this paper synthetic aperture ground penetrating radar (SAGPR) as an imaging technique in oil well is proposed. The system uses an EM short pulse with spectrum from 1.4 to 11 GHz to provide a high resolution in down-range. Cross-range resolution is made by SAR processing [14]. We also used frequency modulation continues wave for EM pulse because of its good autocorrelation properties and since the object being imaged is at-close ranges to the radar [15].

Simulation is based on real data which provided by a complete measurement of dielectric properties of crude oil, oil sand, asphaltene and bitumen by Agilent dielectric probe. The organization of this letter is as follows: in section 4.3the Oil-well structure and system design is demonstrated. Dielectric measurement is presented in section 0. Section 4.5 is dedicated to simulated Data and SAR processing. Simulation results and discussion are presented on this part as well. Finally, section 4.6 gives a conclusion to the work.

4.3 OIL-WELL STRUCTURE AND SYSTEM DESIGN

In this section the structure of the system suitable to monitor the oil well under investigation is explained. All of the simulations are based on parameters that are shown in Fig. 4.1. The oil well diameter is considered to be 20 cm (any other oil–well diameter can be accommodated by adjusting the pulse width that will be described later.). The well is surrounded by the concrete wall without metallic casing. This model represents approximately 30% of the oil well around the world. The oil reservoir is the combination of crude oil, asphaltene, rocks (pressed sand) and oil sands as it is shown in Fig. 4.1.a. An ultra-wideband antenna is located in the oil well toward the walls to scan the near well-bore medium. The antenna is moved along a shaft upward or downward step by step (Fig. 4.1.a) to provide the required apertures for SAR processing. In each step the antenna sends a signal and collects the reflections like mono static radar. The first detected target along the range is the concrete oil well wall surface. The last detected range (Fig. 4.1.b) which is the penetration depth is determined by pulse width and silence time respectively. These parameters are known as the timing of the transmitted pulse and are keys to determine the first and last detected range accordingly.

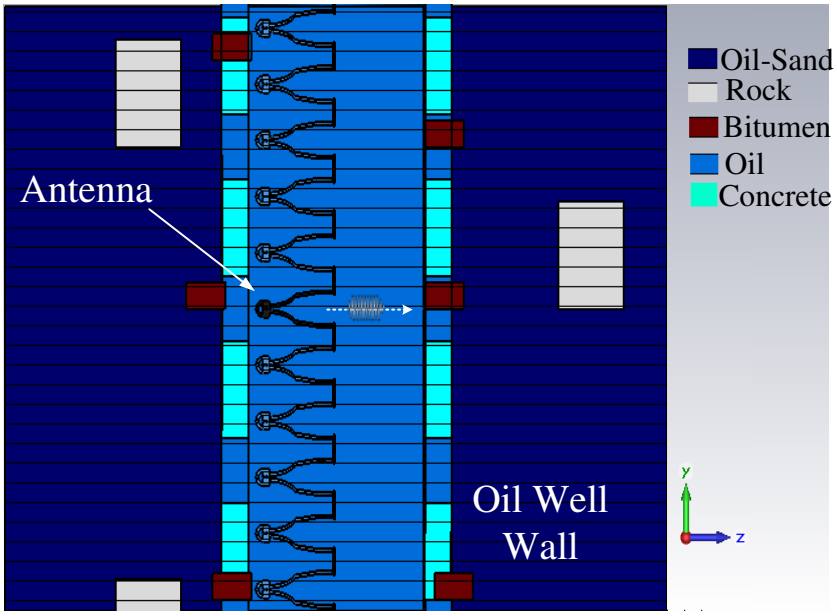

(a)

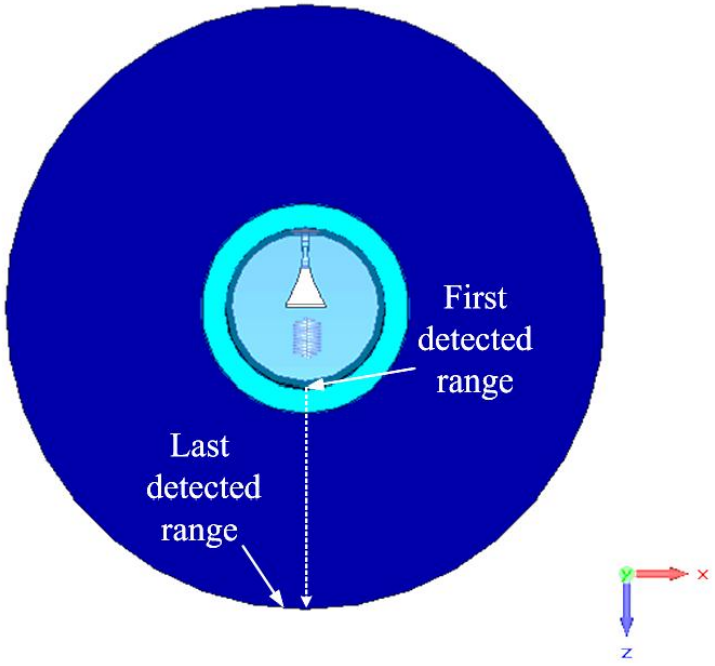

(b)

Fig. 4.1. Oil well monitoring by SAR (a) Side view (b) Top view.

4.3.1 IMAGE RESOLUTION

Image resolution depends on the parameters which are including bandwidth, pulse shape, and the most important one is the method that data is processed to extract the information. A high resolution image needs both range and azimuth resolution. Here depth resolution is the equivalent of the range resolution as defined by common radar systems. The radar ability to distinguish two sequential targets correctly is so called range resolution which is given by:

$$R_a = \frac{\mathrm{c}\, T_p}{2} = \frac{c}{2\ \mathrm{BW}} \quad (1)$$

Where c is light velocity, T_p is pulse width and BW is bandwidth. Therefore, a signal with smaller time interval T_p has more resolution. Fig. 4.2.a. shows range resolution versus bandwidth. As can be observed, as the bandwidth or dielectric constant of the medium increases, range resolution is improved. So if high resolution is needed, wideband spectrum of frequencies should be used.

Azimuthal resolution is the radar's ability to distinguish side-by-side targets clearly. It is related to the antenna beam-width which can resolve two separated targets besides each other. For azimuth resolution, a physically large antenna is needed to produce the narrow radiation beam. The sharpness of the beam defines the azimuth resolution. SAR has the ability to produce high azimuth resolution that differentiates it from other radar systems. A narrow beam resulted from the relatively large synthetic aperture yields a high resolution. The obtainable azimuth resolution by SAR can be expressed as:

$$R_a = \frac{H \cdot \lambda}{L \cdot \cos\theta} \quad (2)$$

In which H, L, λ and θ is altitude, aperture length, wave length and looking angle respectively. As the antenna in this system is looking straight to the well wall, the angle between antenna and object under imaging is zero($\theta = 0$). The azimuth resolution is proportional to $\frac{\mathrm{H}}{\mathrm{L}}$ for different values of λ and $\theta = 0$ as plotted in Fig. 4.2.b. It shows that increasing the aperture length improves the azimuth resolution.

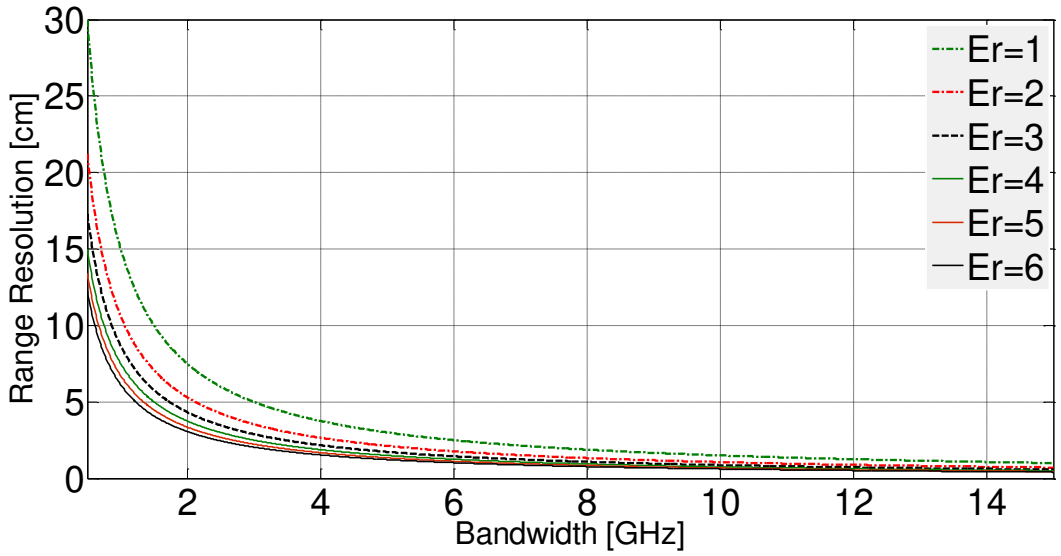

(a)

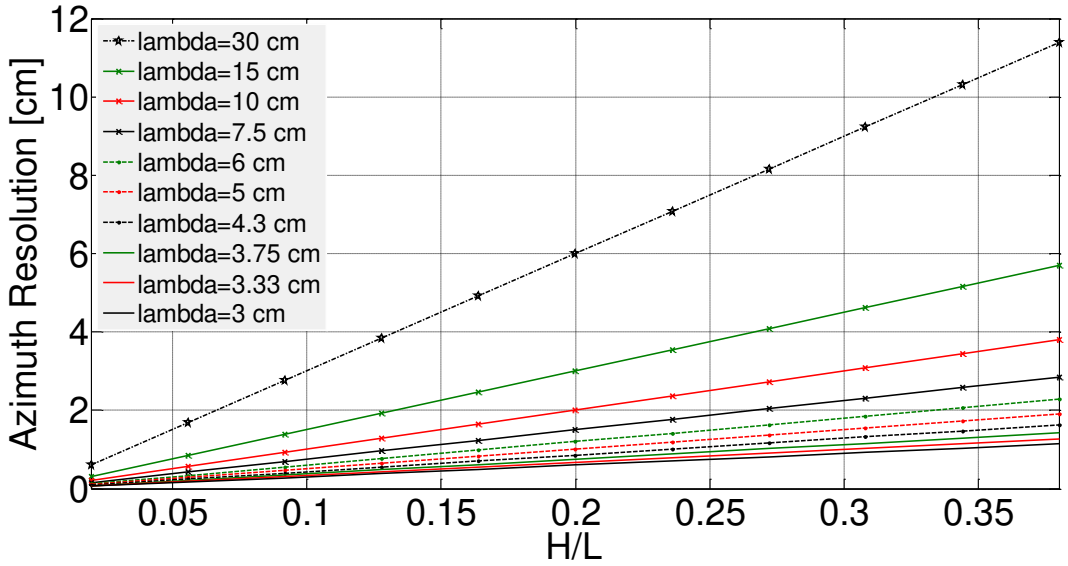

(b)

Fig. 4.2. (a).The range resolution as a function of bandwidth and dielectric properties (b) Azimuth resolution proportional to $\frac{H}{L}$ and wave length (λ).

In the proposed imaging system, a nano-second pulse is employed as the transmitted signal with wide spectrum form 1.4 GHz to 11 GHz to get the depth resolution less than 1 cm. The aperture length L is considered to be 2.5 meter to get azimuth resolution less that 1 mm after SAR processing. Imaging with a UWB signal should be supported by a system with proper designed antenna which can generate images with high range resolution. Therefore a TEM horn antenna with about 8 cm length is also designed that can operate inside oil as transceiver to send

and receive aforementioned pulses [15]. In addition to the UWB signal that is crucial for resolution, signal shape is another factor that can increase resolution with the same bandwidth.

4.3.2 PULSE IMAGING METHOD

As discussed earlier to have high resolution radar image a very narrow pulse in time domain is needed. This pulse is employed to measure distance, reflectivity and shape of the object. Therefore, the required pulse should be strong enough in that short time to produce an accurate measurement. Producing narrow time domain pulse with a high level of power to have high quality measurement especially for far distance is a difficult task in most cases. Instead, to get a high power and fine resolution time domain pulse, some types of signal processing can be used. Pulse compression is a technique to solve this problem [16]. Pulse compression is based on the autocorrelation function of transmitted signal which is known as match filtering. Chirp signal is one of the signals with very good autocorrelation properties.

Before applying match filter, the pulse resolution is equal to transmitted pulse with duration T_p while after conducting the match filter operation over the received pulses with transmitted pulse, the output is approximately a Sinc function with a high resolution in comparison with the chirp pulse. The chirp signal is employed as the transmitted signal in this work. The employed chirp pulse and the corresponding compressed pulse are shown in Fig. 4.3. The real part of normalized amplitude Sinc with real part of chirp signal is depicted in Fig. 4.3.a. The figure demonstrates that the resolution is considerably increased by the same bandwidth after pulse compression. The absolute amplitude of the Sinc is plotted in Fig. 4.3.b. It demonstrates that the amplitude increased to more than 200 times in this case. This is considered as the signal processing gain.

4.3.3 SYSTEM TIMING

System timing plays a very important role in radar systems to define the nearest and farthest range of detection. In radar systems, echo is often received directly after the transmitted pulse and before another pulse is being transmitted. So the time required to detect the first target is equal to the pulse width. The pulse width should be altered in a way that the echoes of the first target arrive after the pulse transmission.

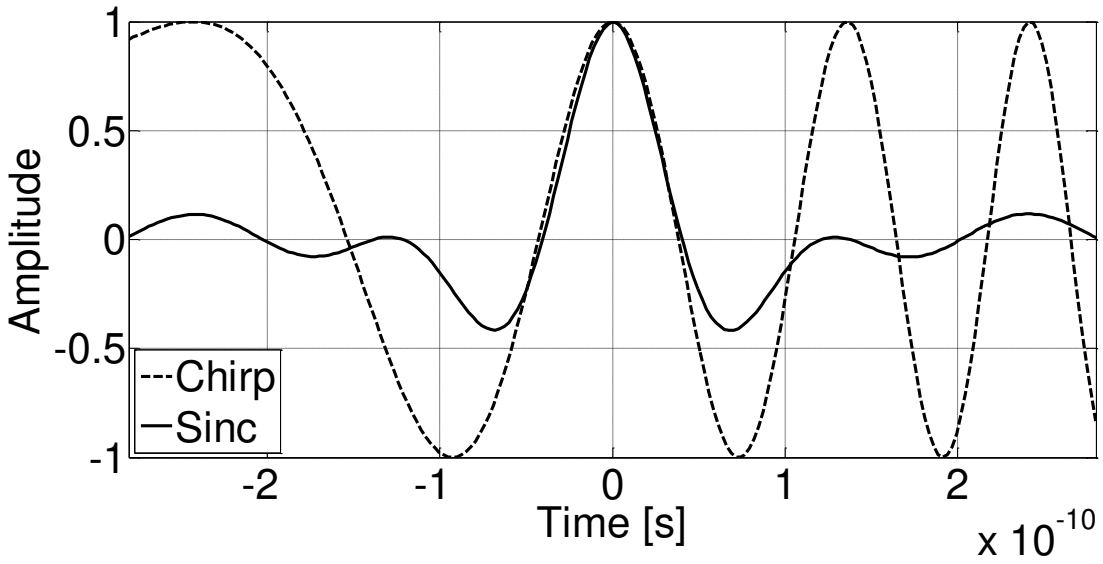

(a)

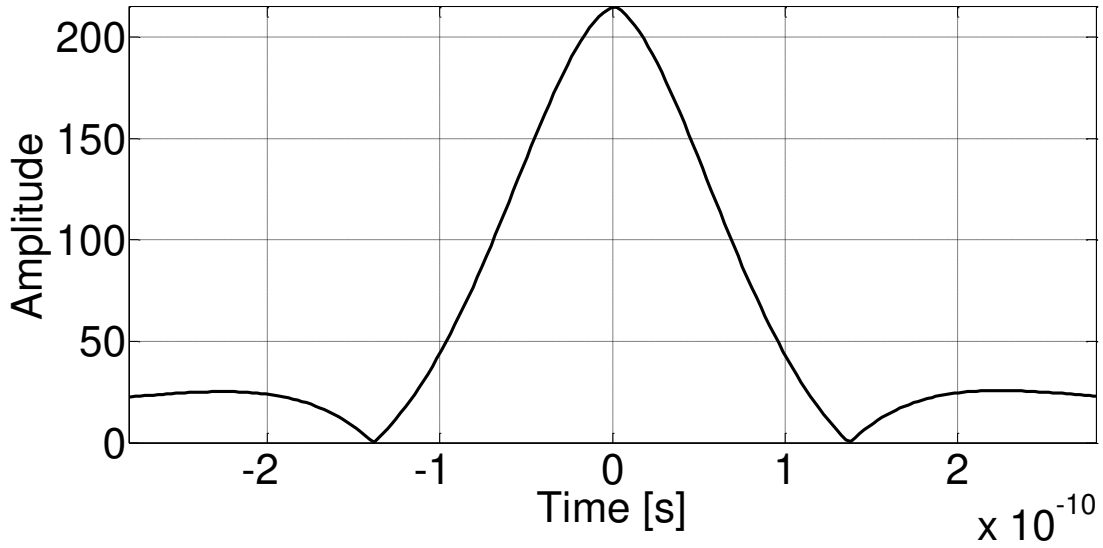

(b)

Fig. 4.3.(a). Real part of chirp and normalized amplitude of corresponding Sinc pulse, (b) Absolute magnitude of corresponding Sinc pulse.

The distance between antenna and target d and propagation velocity v are related to pulse width T_p by:

$$d = v.T_p \tag{1}$$

The silence period is required for the recording the desired echoes. The more silence time results in a more depth or range detection. In this case, the oil well diameter is about 20 cm and the desired penetration depth through the reservoir is 50 cm as most of asphaltene deposition occurs in shallower depth. Deeper depth can be detected just by increasing the transmitted power. The medium permittivity is considered to be about 2.33 for oil and 4 for oil and wall materials respectively for calculation of the pulse width and silence time. The design parameters used for this simulation are shown in Table.1. For other material properties, these numbers can be altered. The pulse width should be short enough to detect the oil well wall surface and the silence time should be big enough as all reflections (multi-path) have to be died out.

Table.1.SYSTEM SPECS

Frequency	Pulse width	Silence time
1.4 to 11 GHz	0.56 ns	15 ns

4.4 DIELECTRIC MEASUREMENT OF CRUDE OIL AND RELATED MATERIALS

Dielectric properties play a very crucial role in ground penetrating radar imaging since all reflections are due to dielectric contrast in the medium which causes the difference in intrinsic impedance in inhomogeneous mediums. Therefore, it is important to determine dielectric contrast between the materials under investigation. Agilent 85070E dielectric probe kit and VNA (E8362B) are used during these measurements. All materials are measured in the same condition. Two layers of RF absorbers (ECCOSORB, FGM) and a layer of foam with 15 cm thicknesses are located between the materials' container and the floor to prevent unwanted reflections from the floor.

The measurement setup is illustrated in Fig. 4.4. The crude oil, oil-sand, asphaltene, bitumen and pressed sand (rock) are measured as shown in Fig. 4.4.a, b, c, d & e respectively. The probe is immersed into or positioned over the materials for measurement. Measurement results for dielectric measurements are depicted in Fig. 4.5 from 0.5 to 20 GHz.

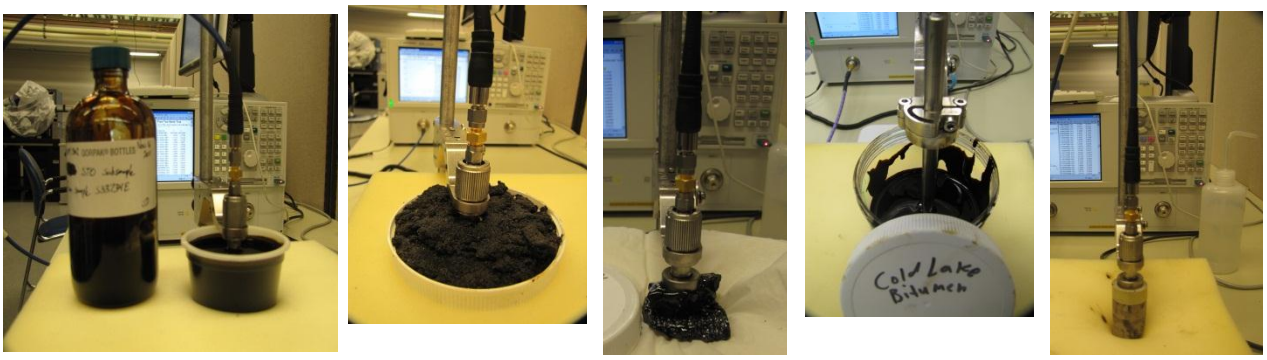

Fig. 4.4. (a) Crude Oil, (b) Oil sand (c) asphaltene (d) Bitumen (e) Sand.

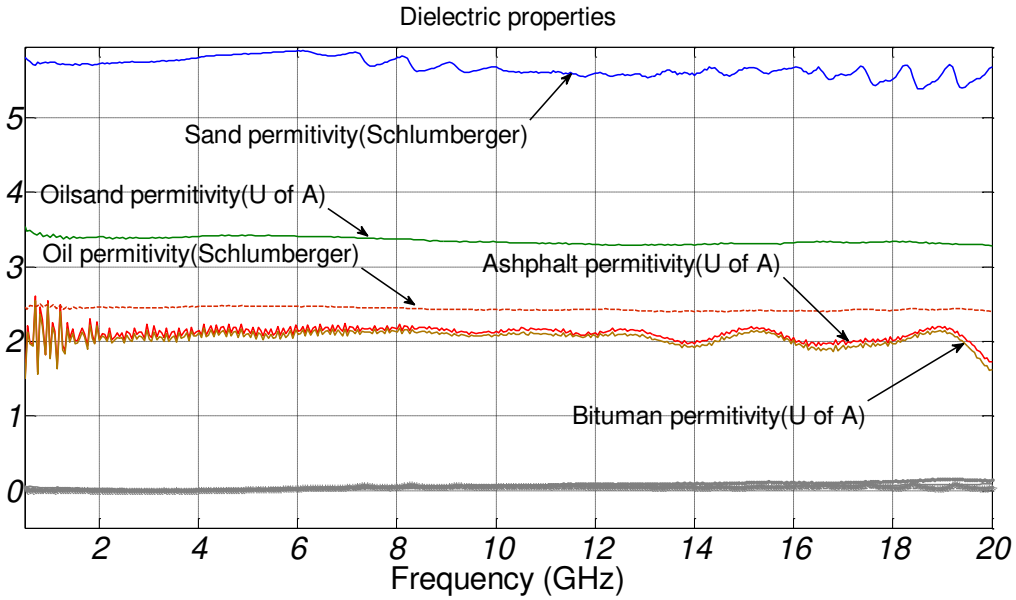

Fig. 4.5.Measurement results for material dielectric properties.

The oil and sand is provided by Schlumberger Company (DBR Technology Center, Edmonton AB, Canada) and other materials by University of Alberta (U of A) Chemical Engineering Department. All the color lines show the relative permittivity while the gray lines correspond to dielectric losses. The sand and asphaltene or bitumen has the highest (5.75) and lowest (2.1) dielectric constant respectively. It is observed that the lowest contrast is also between oil and asphaltene or bitumen. The dielectric properties of materials fluctuate a little by frequency. For the next steps and simulations, the average dielectric constants which are shown in Table.2 are considered.

Table.2.AVERAGE DIELECTRIC CONSTANTS

Crude Oil	Oil sand	asphaltene & Bitumen	Sand	Concrete
2.47	3.4	2.1	5.75	4.5
0.025	0.04	0.05	0.045	0.005

4.5 SIMULATED DATA AND SAR PROCESSING

In order to verify that the oil well materials can be discriminated from each other a simple oil well model is created. Based on measured data of dielectric, a two- dimensional (2-D) oil well with concrete walls is established. The oil well structure is as follow. The oil well medium up to the surface of concrete wall is filled with crude oil (Fig. 4.6.a). After that there is a wall made by concrete with perforations to accommodate the passage of the oil. Inside the reservoir is filled out with oil-sand. Some pieces of pressed sand that are similar to rock in the aspect of dielectric constant are also located inside the oil wells. Moreover pieces of asphaltene or bitumen are located close to the perforations and concrete walls or inside oil sand for the simulation purpose. As it is explained already, asphaltene and bitumen can cause problems by deposition in porous media that leads to well impairment. Therefore, the purpose of this paper is the discrimination of asphaltene from other materials in proposed media. The 2-D oil well model constructed as shown in Fig. 4.6.a. This model is simulated using finite difference time domain (FDTD) method. Any dielectric changes in the medium causes reflected power given by:

$$p = \frac{\eta_2 - \eta_1}{\eta_2 + \eta_1} \tag{2}$$

In which

$$\eta = \sqrt{\frac{\mu}{\varepsilon}} \tag{3}$$

And "η", "μ "and "ε" are intrinsic impedance, permeability and permittivity of the medium respectively. The orange dots depicted in Fig. 4.6.a show the antenna movement along well axis to collect raw data. The raw data is made by sending and receiving pulses in every position. Then received pulses are compressed by match filtering method with transmitted pulse. B-scan radar data is generated by arranging received pulses beside each other from first to last position.

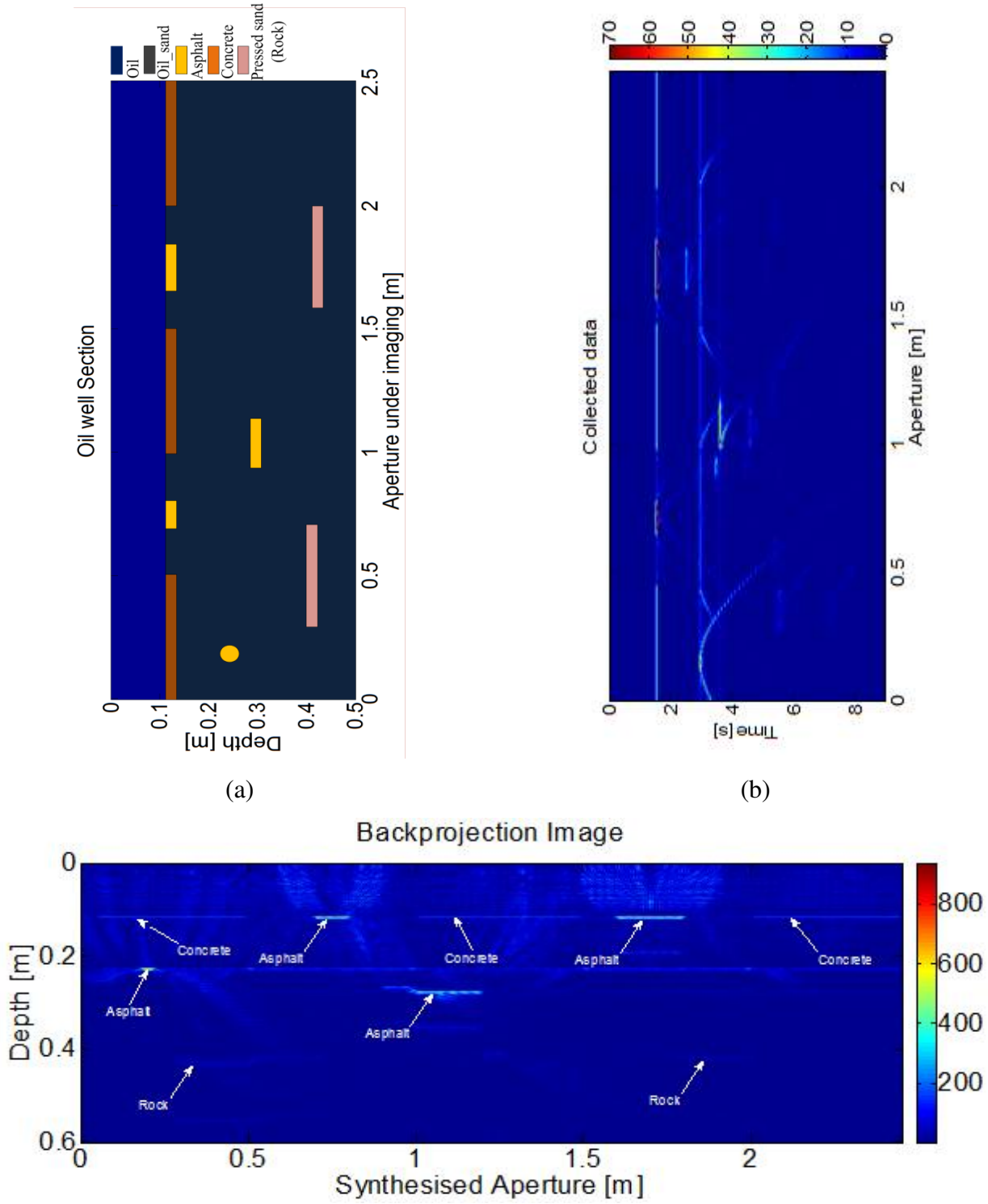

Fig. 4.6. Oil well simulation and data processing (a) 2-D simulated GPR data for Oil well (b) B-scan (raw) data by FTDT (c) Back projected Image .

We considered 151 positions along 2.5 meter aperture. The simulated cross section (2-D) of the oil well size is 2.5m*0.5m.

In order to find an image of different materials in oil well especially asphaltene, a 2-D raw data which is similar to the B-scan ground penetrating radar (GPR) data is derived by simulation as shown in Fig. 4.6.b. The antenna collects 2-D data in spatial and time domain as it moves along the shaft in different positions.

In the next step, the SAR processing is performed, resulting in a 2-D image that shows the locations of different materials. SAR processing of the time-domain GPR data consists of defining the area to be imaged and constructing the SAR image. The time-domain GPR data are in the form of 151-point of time domain pulses after match filtering. The image is constructed by coherently summation (for each pixel in the image grid) of data point from each auto-correlated chirp time-domain waveform corresponding to the round-trip time (delay time) between the antenna and the image grid (image pixel). Moreover, the time needed for pulse compression which is $(\frac{T_p}{2})$ should be added to this calculated time delay as this time was used for match filtering in the processing procedure.

The data from the antenna is in the form of N_X-data . N_r-data in which N_X-data is number of apertures and N_r-data is number of bins in range direction. Interpolation is very helpful to increase the accuracy of selecting correct sample by increasing the number of bins.

The 2-D SAR image is created by summing the appropriate data points from each waveform correspondent to each grid element in the image. The image is constructed by M*N grid plane in direction of *X* (well axis) and *Z* (depth through wall) respectively. Here, M and N are 3001 and 1001 for constructed image accordingly. To find the appropriate data points in time, the wave traveling time for each grid should be calculated. The time is calculated by:

$$t = \frac{D_{total}(M,N)}{v} \quad (44)$$

In which

$$D_{total}(M,N) = 2\sqrt{(X_{pf} - X_M)^2 + (Y_{pf} - Y_N)^2} \quad (5)$$

and

$$v = \frac{C}{\sqrt{\varepsilon_r}} \tag{6}$$

"X_{pf}" and "Y_{pf}" are location of the platform that is carrying the antenna. "c", "ε_r" and "v" are light velocity, dielectric constant and wave velocity in specific medium respectively. The wave velocity plays crucial role in SAR image reconstruction. The wave velocity depends on dielectric constant of the medium as shown in Equation (8). Simulated oil well contains different materials but one dielectric constant value is needed to calculate the wave velocity of the whole medium. This dielectric constant can be called effective dielectric constant of the medium. SAR processing is done by considering different dielectric constant to calculate the wave velocity inside medium for SAR processing and it is found that dielectric constant of 3.7 give more accurate images after processing.

Next step is to find the corrected sample of each aperture position to get the coherent summation at the each image grid. Dividing the summation of round trip time given by Equation (6) plus elapsed time of match filtering by time resolution gives the index of appropriate sample. The appropriate index is calculated by:

$$Index = rond(\frac{t+\frac{T_p}{2}}{\Delta t}) \tag{4-7}$$

Half of T_p is added to the time due to pulse compression as mentioned earlier. Here the importance of interpolation is clarified. The larger sample population increases the probability of getting the correct sample to get the index after rounding. The image is generated through:

$$I(M,N) = \sum_{0}^{L} raw\ data(l, Index) \tag{8}$$

In which, the "l" is the aperture length. The constructed image is shown at Fig. 4.6.c. As can be seen the constructed image is in a good agreement with the oil well model of Fig. 4.6.a. It can be observed all materials are discriminated from each other. Asphaltene is also detected very well as it was the main goal of this work. This processing method can be applied to any kind of time domain raw data of oil well or ground penetrating radar to get images of scanned medium.

4.6 CONCLUSION

An oil well monitoring system by synthesizing the apertures combined by UWB radar concept is presented in this paper. The system is designed for detection of near-wellbore damages caused by asphaltene or bitumen. The results show that both range and azimuth resolution can be achieved by employing UWB radar with SAR processing. The SAR processing gives the azimuth resolution which is very hard to get in these narrow holes as a high directive antenna is needed for such a purpose. This system provides an image with a very high resolution so that different material could be detected completely with low dielectric contrast. This technique can be a promising solution for oil and gas industries to maintain the oil well production.

4.7 REFERENCES

[1] F. Civan, Reservoir Formation Damage. 2nd ed., Gulf Professional Publishing, 2007.

[2] B. E. Hornby and D. J. Rossi, "Single well sonic imaging of near borehole structure," in Proc. 6th Multidimensional Signal Process. Workshop, Pacific Grove, CA, Sep. 1989.

[3] H. Alboudwarej, K. Akbarzadeh, J. Beck, W. Y. Svrcek, and H. W. Yarranton, "Regular Solution Model for Asphaltene Precipitation from Bitumens and Solvents," 11 AIChE Journal,. Vol. 49, No., Nov.2003.

[4] P. Cheung, A. Hayman, R. Laronga, G. Cook, P. Goetz, M. Marshall, S. Hansen, M. Lamb, B. Li, M. Larsen, M. Orgren, and J. Redden, "A clear picture in oil-base muds," Oilfield Rev., Vol. 13, No. 4, pp. 2–27, 2001.

[5] Y. H. Chen and M.L. Oristaglio, "A modeling study of borehole radar for oil-field applications," GEOPHYSICS, Vol. 67, No.5, pp. 1486–1494.

[6] M. Sato and R. Thierbach, "Analysis of a borehole radar in cross-hole mode," IEEE Trans. Geosci. Remote Sens., Vol. 29, No. 6, pp. 899–904, Nov. 1991.

[7] S. Liu and M. Sato, "Electromagnetic logging technique based on borehole radar," IEEE Trans. Geosci. Remote Sens., Vol. 40, No. 9, pp. 2083–2092, Sep. 2002.

[8] T. M. Habashy and J. Xia, "Borehole logging tools and methods using reflected electromagnetic signals," U.S. Patent 5 530 359, Jun. 25, 1996.

[9] D. L. Wright, R. D. Watts, E. Bramsoe, "A short-pulse electromagnetic transponder for hole-to-hole use," IEEE Trans. Geosci. Remote Sens., Vol. GRS-22, No. 6, pp. 720–725, Nov. 1984.

[10] Y.H. Chen and M. L. Oristaglio, "Borehole radar for oil-field imaging: A study based on numerical modeling," Schlumberger–Doll Res., Ridgefield, CT, Int. Res. Rep., 1998.

[11] W. C. CHEW, "Modeling of the Dielectric Logging Tool at High Frequencies: Theory," IEEE Trans. Geosci. Remote Sens., Vol. 26, No. 4. , pp. 382-387 July I998.

[12] C. Guo and R. C. Liu, "A Borehole Imaging Method Using Electromagnetic Short Pulse in Oil-Based Mud," Geosci. Remote Sens., Lett. Vol. 7, No. 4, pp. 856–860, Oct. 2010.

[13] Soumekh, Mehrdad. Synthetic Aperture Radar Signal Processing with Matlab Algorithms, John Wiley & Sons, Inc., 1999.

[14] F. Sender, "Borehole antenna array for determining radar incidence direction," U.S. Patent 4670717, Jun 2, 1987.

[15] A.S. Turk, "Ultra wideband TEM horn design for ground penetrating impulse radar system," Microwave *Optical Technology Lett.*, Vol. 41, No. 5, pp. 333–336, June 2004.

[16] D. Oloumi, M.I. Pettersson, D. Elliott, P. Mousavi, "A TEM Horn Antenna with Non-uniform Expansion for Oil Well Monitoring," accepted to be presented at antenna and propagation symposium, .Chicago, 2012.

Part II

"A Modified TEM Horn Antenna Customized for Oil Well Monitoring Applications"

Part II:

D. Oloumi, P. Mousavi, M.I.Pettersson, D. Elliott, "A Modified TEM Horn Antenna Customized for Oil Well Monitoring Applications," IEEE Transactions on Antennas and Propagation, submitted for publication.

A Modified TEM Horn Antenna Customized for Oil Well Monitoring Applications

5.1 ABSTRACT

A TEM horn antenna with modified radiation pattern customized for oil well monitoring application is presented here. The antenna is designed to work from 1.4 to 11 GHz in oil medium. A complete design procedure for the antenna that modifies radiation pattern performance by preserving return loss is explained in this paper. The modification is conducted using non-uniform expansion for antenna flares. Through this technique the mainlobe radiation pattern ripples at higher frequencies which are the problem of conventional TEM horn antenna are removed. The expansions coefficient is optimized using CST Microwave Studio to achieve better than 10dB return loss and smooth radiation pattern in the main beam. The designed structure is validated by fabrication and measurement of proposed TEM horn antenna. Fabricated antenna dimensions including balun is limited by 89.2×49.2×78.2 mm. Radiation pattern measurements are done in free space in frequency bandwidth of 2.2 to 18.6 GHz. Simulation results are followed by measurement results with a very good agreement. The designed antenna is utilized as a part of an ultra-wideband radar system for oil well monitoring.

5.2 INTRODUCTION

Reservoir management is considered by geophysicists and petrophysicist as one of the most important tasks nowadays. The required information about formation evolution to make more certain decisions can be derived using borehole imaging [1]. Formation damage inside oil wells is a generic terminology referring to the impairment of the permeability of petroleum- bearing formation by various adverse processes [2]. Several methods have been used for this problem,

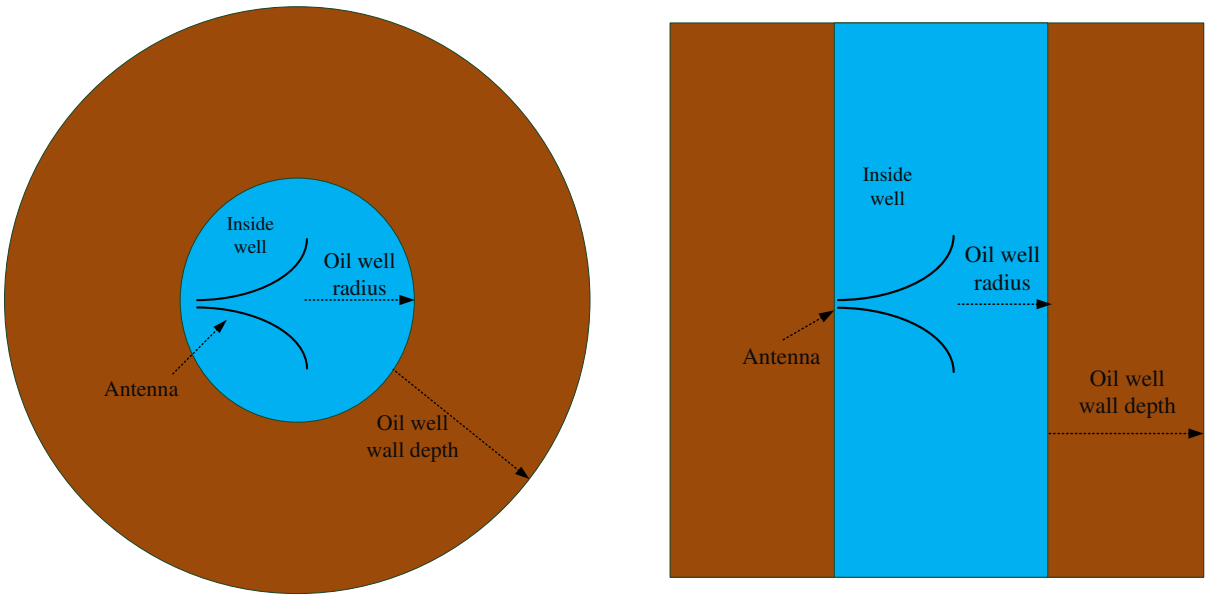

Fig. 5.1. Oil well structure (a) top view, (b) side view.

but UWB radar imaging techniques such ground penetrating radar show a great promise as a solution to monitor underground reservoirs and material composition in oil wells [3, 4].

Ultra wide band antennas are the most important parts of these systems to achieve high resolution images. Bow-tie, Vivaldi, spiral, double ridged and TEM horn antenna are examples of UWB antennas that have been incorporated in many different radar systems. Transverse electromagnetic (TEM) horn antennas have been popular for variety of other application like ultra-wide band communications and pulse radiation applications due to their characteristics including UWB impedance matching, unidirectional radiation, low dispersion, and low distortion [5-10].

In this application, TEM horn antenna is utilized as a transceiver of an UWB penetrating radar system which is placed normal to the oil well wall to image within oil well structure as shown in Fig. 5.1. The oil well wall is constructed by concrete, oil sands, perforations, asphaltene and etc. Electromagnetic waves through antenna illuminate the well walls. Scattered reflections collected by antenna will be processed to evaluate well wall material properties.

TEM horn antenna can be considered as an impedance transformer made by a pair of parallel plates to match the transmission line to the medium of propagation. Shaping of TEM horn antenna plates to continuously transfer the input impedance to the media of propagation

impedance is first proposed by [11]. This transformation can be realized by using uniform exponential, Chebyshev, Hecken or elliptic profiles [12-15].

The main problem with most UWB TEM horn is the fluctuation of the mainlobe of the radiation pattern over the high frequencies. This is problematic in many applications. Some approaches such as removing part of the antenna body or changing the antenna shape are proposed by [13, 14] respectively to mitigate this problem.

In this paper a TEM horn antenna with modified radiation pattern capable of radiating into oil well walls with an optimum aperture is realized. The design goal is enhancing antenna radiation pattern while preserving the return loss in oil media. Non- uniform expansion for antenna flares is proposed as a solution of TEM horn antenna radiation pattern problem [16]. Limited size of oil well puts some constrains on antenna design to reach the required frequency bandwidth. Two rectangular sheets are also attached to the end of both flares to improve antenna return loss in lower frequencies as well.

Paper structure is as follow, TEM horn antenna modification methodology is discussed in section 5.3. Designed modified TEM horn antenna and balun design is explained in Sections 5.4 and 0. Simulation and Measurement Results are discussed in section 5.6. As mention before this antenna works in a radar system. The antenna performance in GPSAR system is shown in section 5.7. Last section (5.8) is the conclusion to the presented work.

5.3 TEM HORN ANTENNA MODIFICATION METHODOLOGY

TEM horn antenna is a parallel plate waveguide that acts as an impedance transformer. The uniform exponentially tapering in two directions for a conventional TEM horn antenna works as an impedance transformer from feeding point to the medium of propagation [12]. One drawback of such a conventional TEM horn antenna is that the uniform tapering causes the ripple in the mainlobe at higher frequencies [13-14]. This phenomenon happens due to the phase difference between field at aperture center and end of flares as shown in Fig. 5.2.a. The phase difference is calculated by:

$$\phi = \frac{2\pi}{\lambda}.d \tag{1}$$

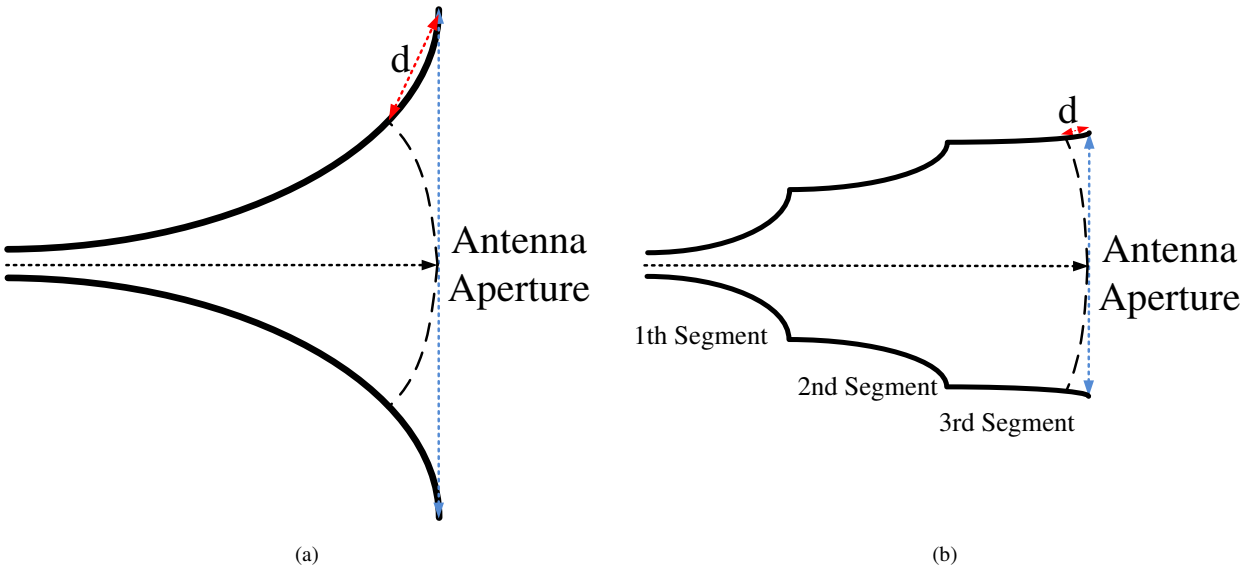

Fig. 5.2 .TEM horn antenna, (a) Conventional, (b) Modified

In which λ and d are wave length and distance accordingly. This phase difference is significant at higher frequencies since phase difference grows up as frequency increases according Equation (1). Large amount of phase difference at high frequencies causes the out of phase far field summation that produces the ripples or notches in antenna mainlobe radiation pattern. One way to reduce the phase difference is to make antenna flares as parallel as possible to each other at the aperture cross-section .In this way d is reduced that consequences in zero phase difference. As the TEM horn is an impedance transformer, the main challenge is to find a profile to transfer the impedance that can achieve a smooth radiation pattern while preserving the impedance. As demonstrated in [13], TEM horn antenna flare expansion is uniform exponential curve to change the impedance as gradually as possible to minimize the return loss. Therefore, this impedance transformation can be done by any different profile.

We propose a non-uniform exponential tapering for TEM antenna that can mitigate this effect. By non-uniform exponential tapering through different segments as depicted in Fig. 5.2.b, the feed impedance is transferring to the medium impedance while the distance d is going to be decreased to improve the radiation pattern by reducing phase difference.

The TEM horn antenna input impedance depends mainly on the current distribution close to the feed point. Therefore first segment (Fig. 5.2.b) is designed to transfer the main portion of impedance. The other segments have less effect on the impedance transformation which allows for smaller profile slope. This means that a different expansion coefficient (Fig. 5.2.b) can be

considered for different segments to bring the flares parallel to each other at the end to decrease phase distortion without affecting the input impedance.

The antenna is expected to be immersed in an oil medium with relative permittivity of 2.33 operating in the frequency range from 1.4 to 11 GHz to provide requirements for a high resolution radar imaging system. The lower band is chosen according to well diameter and the upper band is considered in a way that enables radar system to work with UWB pulse. The oil well diameter in this case considered being 20cm but it can be changed for different oil well diameters. This requires an antenna with the length of about 8 cm to have a reasonable distance between antenna aperture and well wall surface.

To design the modified antenna, first a conventional TEM horn antenna is designed with uniform expansion, and then the antenna is divided into *n* segments with different expansion coefficients. These coefficient decreases by progression of the segments toward the aperture. The modified antenna is fed by a U-shape cavity as a balun.

5.4 MODIFIED TEM HORN DESIGN PROCEDURE

The initial point to design the modified TEM horn antenna is a conventional TEM horn antenna that is explained in [12, 13]. As it is mentioned in the previous section, the aim is to make the antenna plates parallel to each other at the antenna aperture. To realize the proposed solution the antenna length is divided into three segments with different coefficient to grow the flares. The conventional antenna is grown in two directions of *x* and *y* to propagate in z direction. Therefore, each segment has two growth coefficients of α and β for *y* and *x* axis accordingly. The values for α and β become smaller by progression of segments toward aperture which realizes modified structure as illustrated in Fig. 5.3. The $\alpha_{1,\ 2\ \&\ 3}$ and $\beta_{1,\ 2\ \&\ 3}$ which are corresponding to each segment coefficient are determined such way to minimize mainlobe ripple while preserving the return loss.

These coefficients are optimized by different parameter sweeps. As mention earlier, initial coefficients are obtained from a conventional horn antenna. The first segment should have the sharper slope than the conventional one then other coefficient decreases by one after the other. At the end to use the available space in well efficiently, a rectangular sheet is capped to the end of

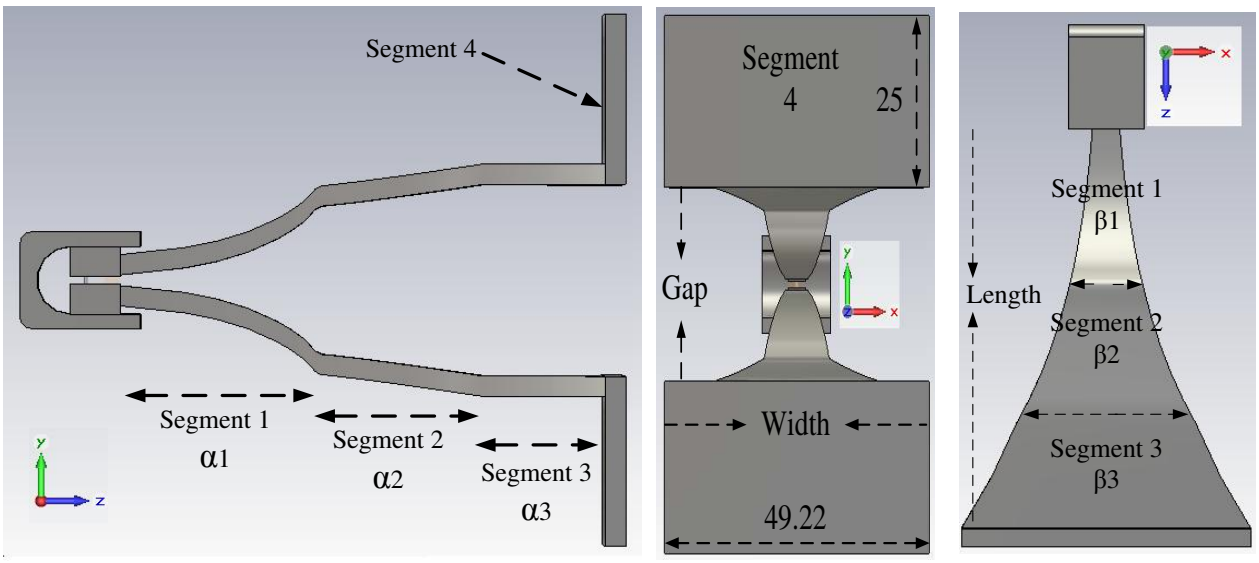

(a) (b) (c)

Fig. 5.3. Modified antenna structure view (b) side (c) front (d) top

flare as the forth segment to increase the antenna length that enables antenna working in lower frequencies for more penetration depth. Table.1 shows the optimized values of α and β.

Table.1. GROWTH COEFFICIENTS

Coefficient/Segment	1	2	3
α	1.27	1.027	1
β	1.1	1.01	1.054

As can be seen the value of α for the third segment is 1 that shows two plates are parallel to each other at last segment. This makes *d* equal to zero which means the phase difference is removed. It is worthy to mention that as α is decreased to make the plates parallel so β also needs to be decreased to maintain the impedance matched. Table.2 shows modified antenna dimensions after several parameter sweeps to optimize the structure for the best results. *S*, *G*, *W* and *L* are stand for segment, gap, width and length as shown in Fig. 5.3. Each segment has 10 sections. All dimensions are in millimeter.

Table.2. MODIFIED ANTENNA DIMENSIONS

	First segment			*Second segment*			*Third segment*		
S	***G***	***W***	***L***	***G***	***W***	***L***	***G***	***W***	***L***
0	0.78	4.1	0	10.81	12.29	29.4	14.11	30.46	53.4
1	0.99	4.53	2.7	11.10	13.46	31.8	14.11	32.13	55.4
2	1.26	5.00	5.4	11.40	14.74	34.2	14.11	33.88	57.4
3	1.59	5.53	8.1	11.71	16.14	36.6	14.11	35.74	59.4
4	2.03	6.11	10.8	12.03	17.67	39	14.11	37.70	61.4
5	2.57	6.75	13.5	12.35	19.35	41.4	14.11	39.76	63.4
6	3.27	7.46	16.2	12.69	21.19	43.8	14.11	41.94	65.4
7	4.15	8.24	18.9	13.03	23.20	46.2	14.11	44.24	67.4
8	5.27	9.11	21.6	13.38	25.40	48.6	14.11	46.66	69.4
9	6.70	10.07	24.3	13.74	27.81	51	14.11	49.22	71.4
10	8.51	11.13	27	10.81	12.29	29.4	14.11	51.91	73.4

5.5 BALUN DESIGN

In many cases, coaxial cable is used to feed the TEM horn antennas. Since the TEM horn antenna is a balance structure, a balun is needed to connect antenna to coaxial line. The balun provides symmetrical modes to excite the antenna for symmetrical radiation pattern. Here U-shape balun is used [14] as shown in Fig. 5.4. The balun should be designed in a way to obtain low levels of return loss as antenna return loss is critically depends on cavity performance. The cavity radius or the distance from feed to short plate should be around quarter wave length at the center frequency to produce in-phase reflection with excitation fields at feed point. Then the distance from short plate should be optimized to minimize the return loss. Moreover the role of ridges is incredibly important as well for impedance matching between antenna and cavity.

After designing an initial structure for both antenna and feed part they should be connected to each other for final tuning. The final dimensions for antenna feed are illustrated in a & b.

5.6 SIMULATION AND MEASUREMENT RESULTS

In this section the simulated and measured results of the modified TEM horn are discussed. The proposed structure is simulated using CST Microwave Studio. For the sake of comparison, a

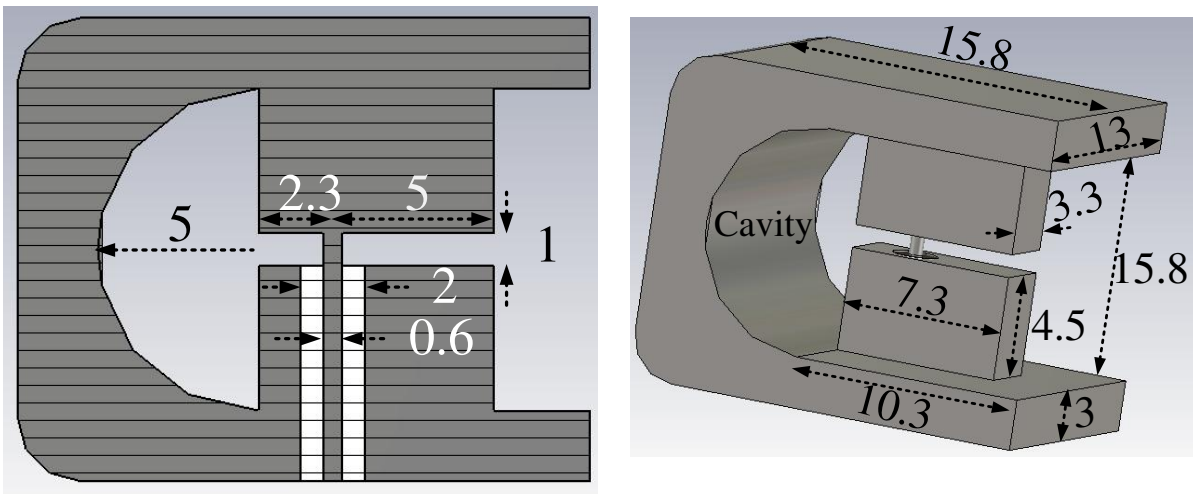

(a) (b)

Fig. 5.4. Feed structure views; (a) side view and (b) Perspective view

conventional TEM horn with same length of modified structure is designed in oil medium. A complete comparison is done between conventional and modified antenna. Convectional antenna size is 82, 79.5 and 86.5 for width, height and length respectively. Conventional antenna radiation pattern is illustrated in Fig. 5.5 in linear scale. As can be seen (Fig. 5.5.a & b) the fluctuations and deeps occur at higher frequency range (8 and 11 GHz). Another issue with this conventional antenna is the asymmetric radiation pattern in E & H planes. It is more obvious in 3 dimensional (3-D) radiation pattern depicted in Fig. 5.5.c & d. These problems are attributed to phase difference that explained earlier. Antenna reflection coefficient is shown in Fig. 5.5.e. As can be seen antenna the reflection coefficient at lower frequencies (from 1.4 to 1.8 GHz) is above -10 dB which is related to the antenna length.

The radiation pattern of the modified TEM horn antenna is shown in Fig. 5.6. Again, radiation patterns are plotted in linear scale and Cartesian coordination so that all small ripples can be observed easily. It is demonstrated (Fig. 5.6.a &b), there are no visible ripples in the mainlobe at higher frequencies and also radiation pattern is symmetric in both E & H plane (Fig. 5.6.c). This method in comparison with other proposed methods [13-14], demonstrates better radiation pattern with simpler structure. Modified antenna reflection is shown in Fig. 5.6.e. This plot demonstrates that growing up the opening flare with non-uniform expansion coefficient does not have negative effects on antenna reflection coefficient which is lower than -10dB in the frequency band. Moreover, antenna reflection is improved at lower frequencies which are the

effect of rectangular sheets caped to the end of flares. It can be considered as length reduction as well which is crucial for borehole radar antennas.

Based on the parameters of last section a prototype of the modified horn is fabricated as shown in Fig. 5.7.a. Due to small dimension of ridges, small SMA connector is used.

The antenna radiation patterns and S-parameters are measured in free space and compared with free space simulation. Antenna S_{11} in air is exhibited in Fig. 5.7.b. The measured and simulated S_{11} are in a very good agreement. Radiation patterns are measured in both H and E planes. Fig. 5.8 and Fig. 5.9 illustrate the antenna radiation pattern simulation in dB scale for E and H plane respectively. Measured radiation patterns are depicted right below the simulations. As can be seen simulations are confirmed by measurement results. The measurement results confirm that this method is a very promising method and a good remedy for TEM horn antenna problem. This method can be applied to other type of TEM horn antenna as well.

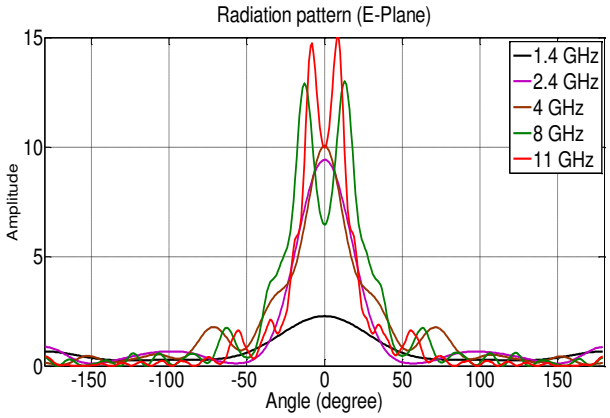

(a)

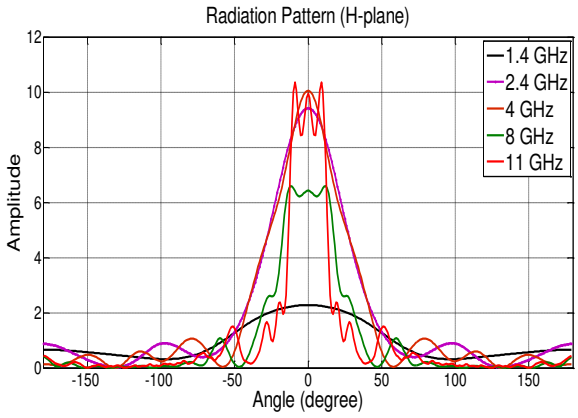

(b)

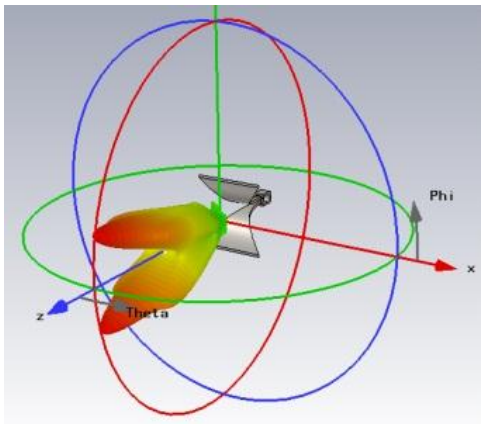

(c)

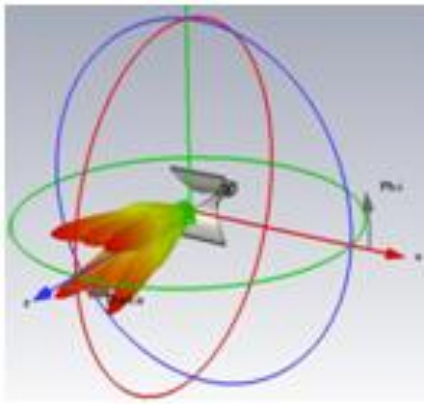

(d)

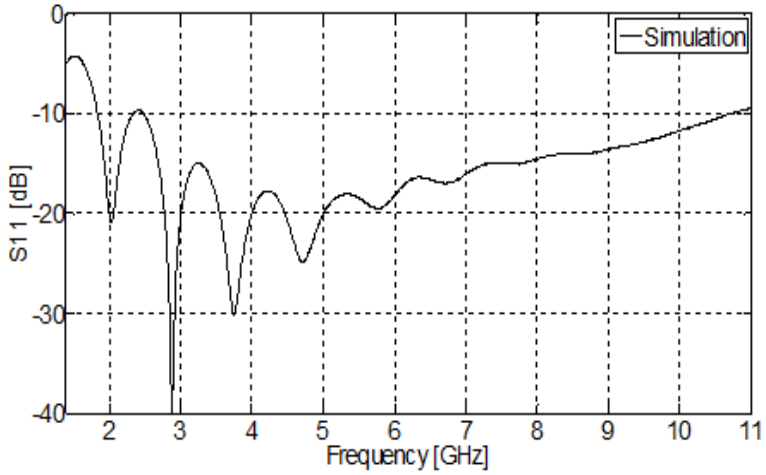

(d)

Fig. 5.5. The conventional TEM horn antenna; 2-D radiation simulatedpattern (a) E-plane, (b) H-plane; 3-D simulated radiation pattern (c) 8GHz and (d) 11GHz; and (e) the simulated antenna S_{11} in oil.

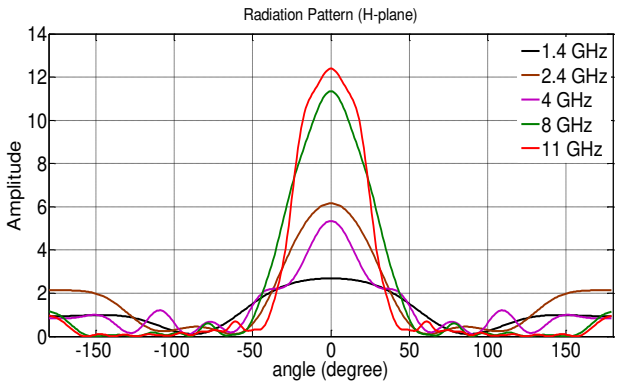

(a)

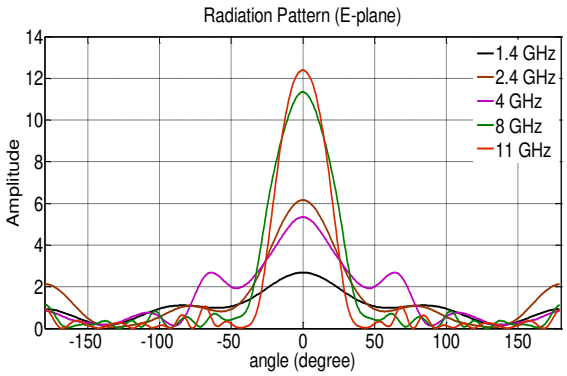

(b)

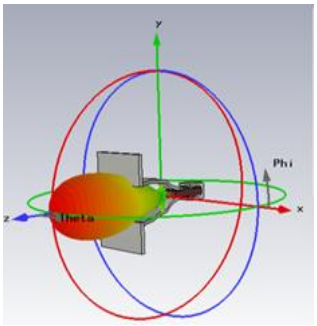

(c)

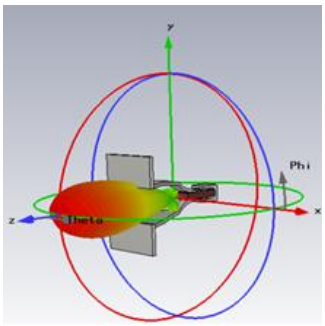

(d)

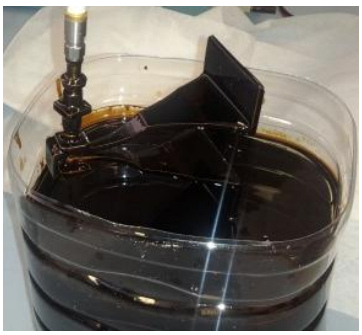

(e)

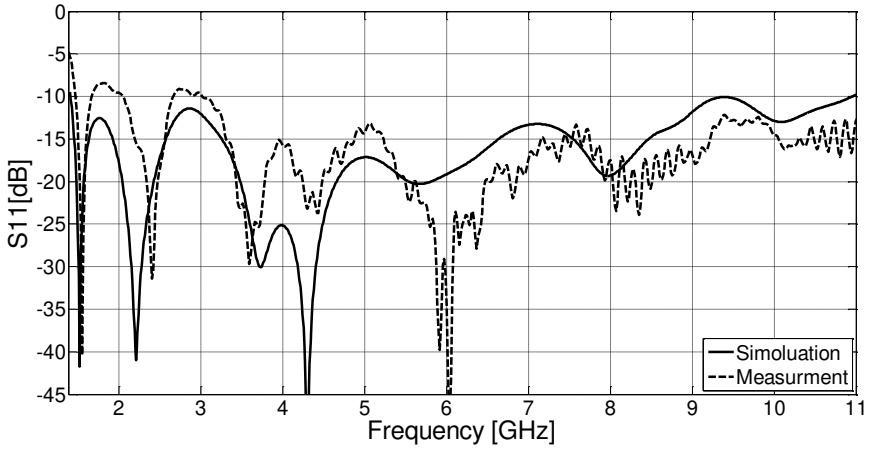

(f)

Fig. 5.6. The modified TEM horn antenna; 2-D simulated radiation pattern (a) E-plane, (b) H-plane; 3-D simulated radiation pattern (c) 8GHz and (d) 11GHz; (e) the antenna s_{11} measurement setup, and (f) the antenna simulated and measured S_{11} in oil.

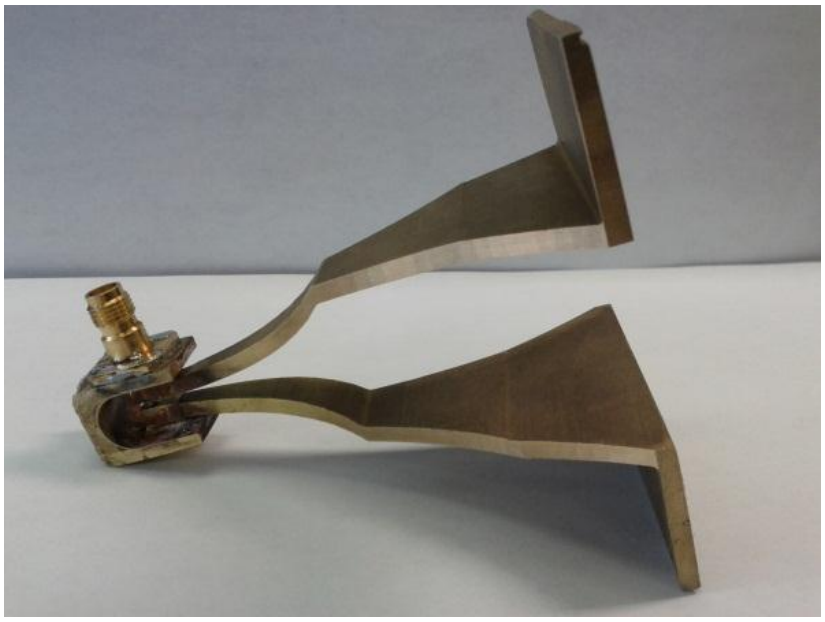

(a)

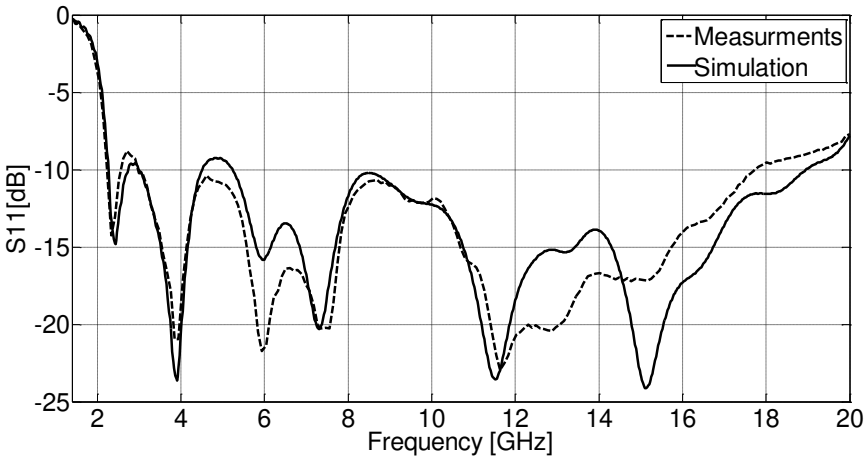

(b)

Fig. 5.7. (a). Fabricated antenna, (b) antenna S_{11} in air.

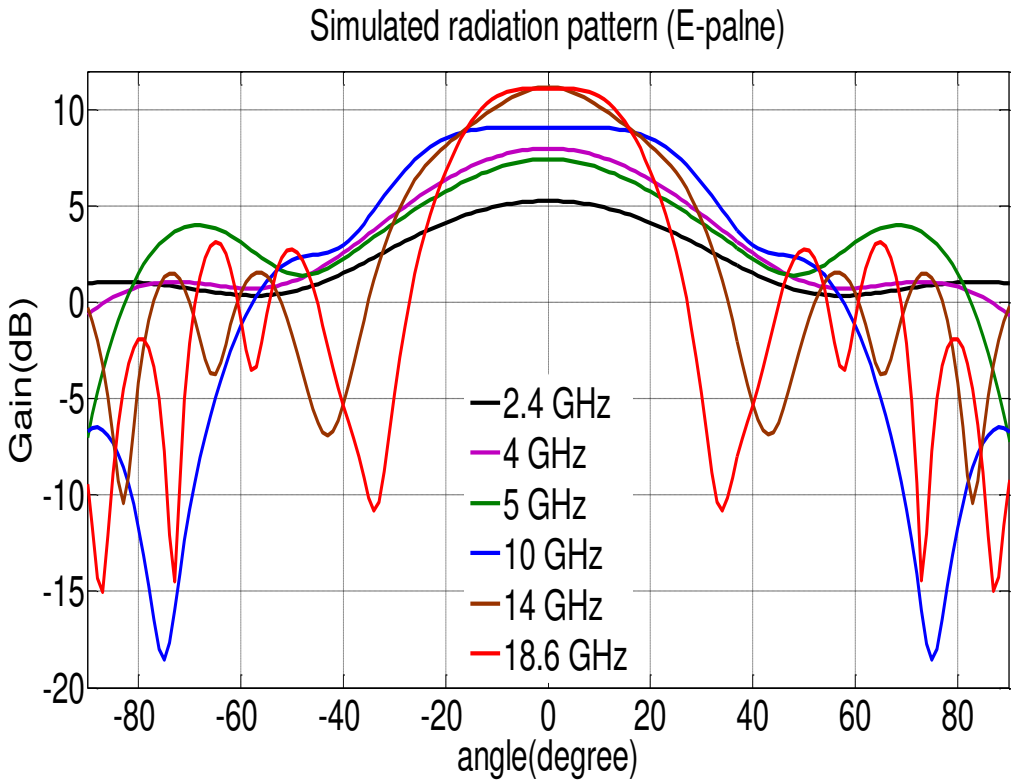

(a)

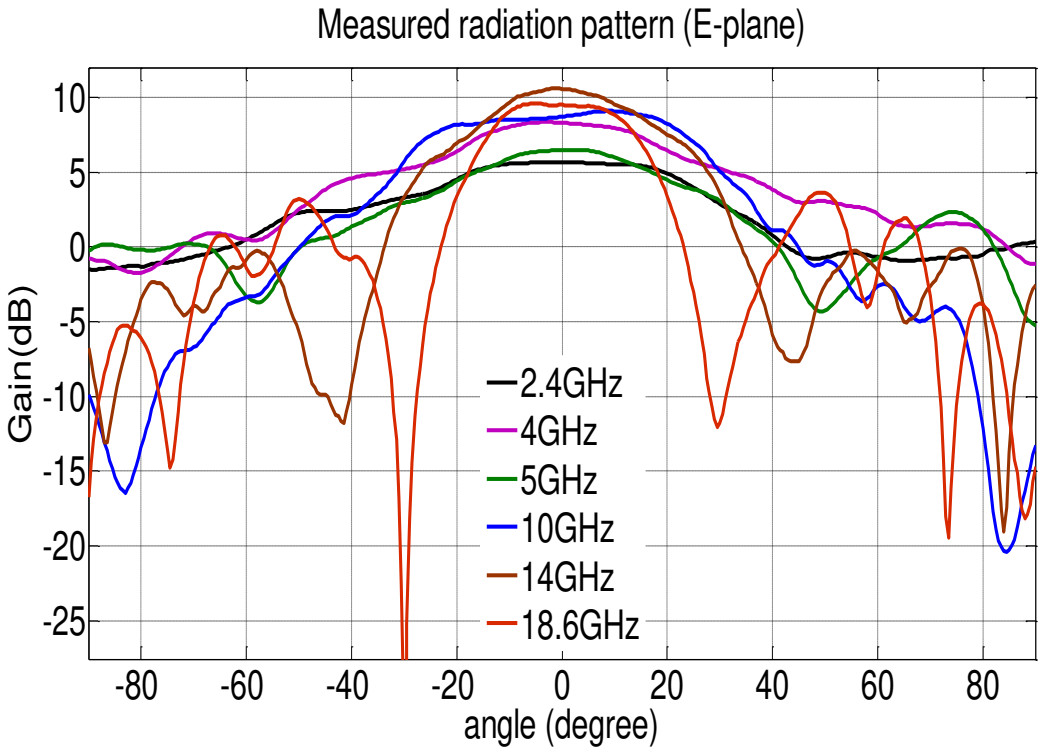

(b)

Fig. 5.8. Antenna radiation pattern in free space, E-plane (a), Simulation (b) Measurements.

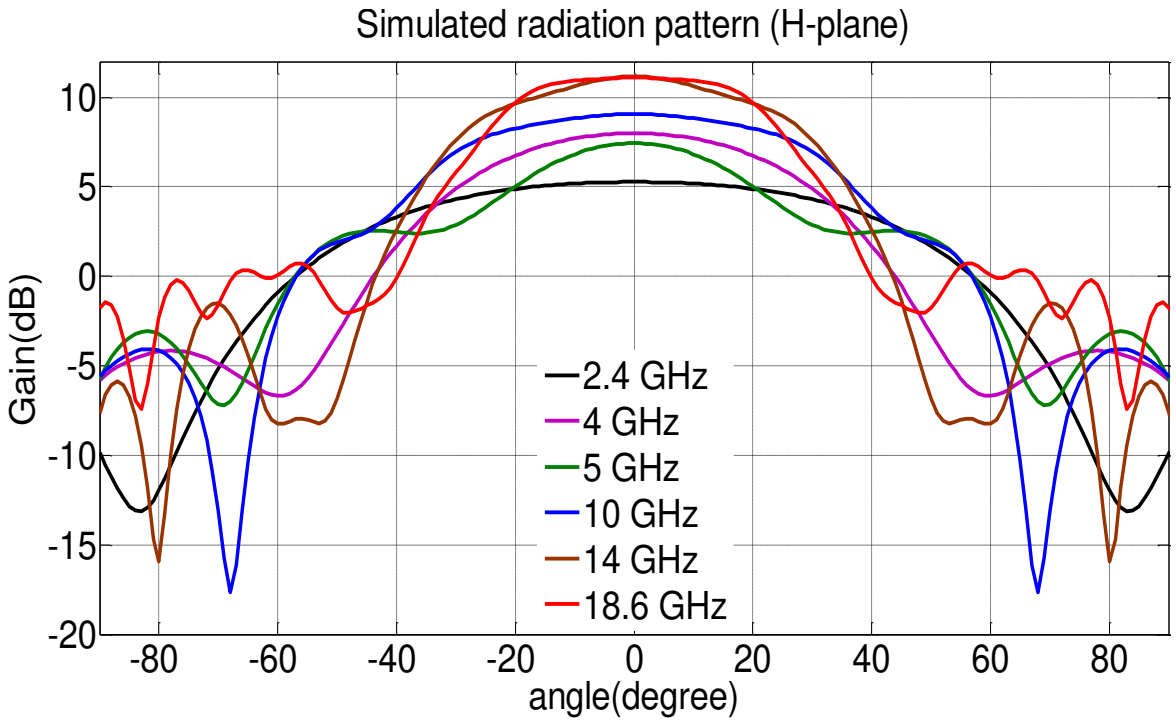

(a)

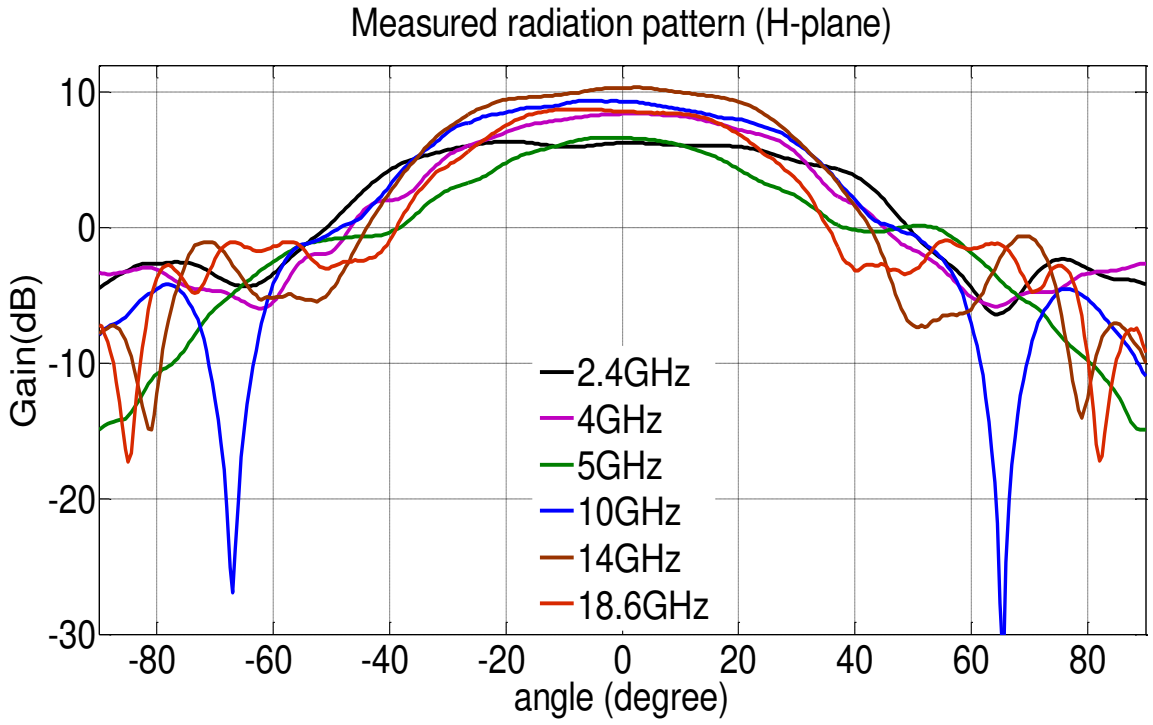

(b)

Fig. 5.9. Antenna radiation pattern in free space, H-plane (a), Simulation (b) Measurements

5.7 ANTENNA PERFORMANCE IN GPSAR SYSTEM

This antenna is employed as a sensor in ground penetrating synthetic aperture radar (GPSAR) system to monitor the oil well (Fig. 5.10). To simulate the antenna performance, a cross section of an oil well with half of meter length and 0.2 m depth is simulated. The oil well is filled by oil sand and three piece of Asphaltene, Concrete and rock which are common materials in oil well. Electrical properties of these materials which are measured by Agilent dielectric probe are in Table.3.

Table.3. DIELECTRIC CONSTANTS

	Crude Oil	Oil sand	Asphaltene & Bitumen	Sand	Concrete
Dielectric constant	2.47	3.4	2.1	5.75	4.5
Loss	0.025	0.04	0.05	0.045	0.025

Simulated oil well is shown in shown in Fig. 5.10. The distance between antenna aperture and oil well surface is 12 cm. A very narrow Gaussian pulse about 0.2 ns pulse width is sent to illuminate the area. The antenna scanned the oil well along well length for 51 positions. The raw data after pulse compression [17] is shown in Fig. 5.11.a.

Image reconstruction is done by using synthetic aperture radar processing (SAR) of raw data (Fig. 5.11.a). SAR processing is done in time domain using global back projection [18]. Through this method, spread energy over hyperbolas is focused by SAR processing of the raw data. After the processing, time in range direction is translated to depth as well. As it is shown in Fig. 5.11.b, all materials are detected completely.

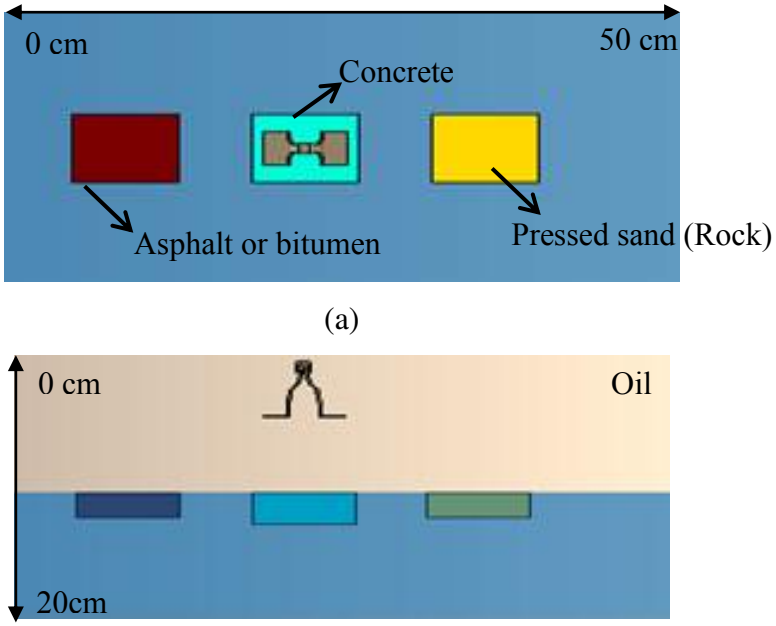

Fig. 5.10. Simulated oil well with modified antenna (a) Top view (b) side view

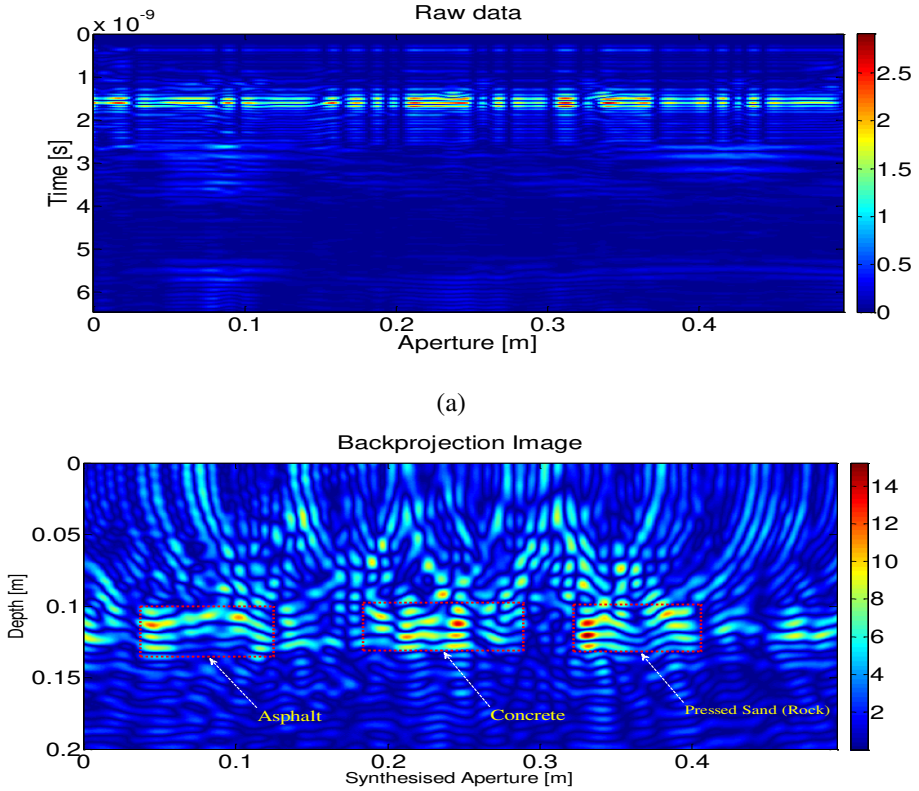

Fig. 5.11. (a) Raw data, (b) Backprojected image using synthetic aperture radar processing.

5.8 CONCLUSION

This paper introduced a method that can remove the TEM horn antenna mainlobe ripple. The full wave simulation shows that the non-uniform expansion is an effective solution to remove the ripple in the mainlobe while preserving the return loss. The proposed structure fabricated and measure. Measurements results follow the simulations by good trend. The designed antenna is customized to work in oil based medium as an UWB sensor for high resolution radar imaging. Constructed image using raw data provided by modified antenna shows that antenna has an acceptable performance to work in a radar system for oil well monitoring.

5.9 REFERENCES

[1] P. Cheung et al., "A clear picture in oil-base muds," *Oilfield Rev*, 2001, Vol. 13, No. 4, pp. 2–27.

[2] F. Civan," *Reservoir Formation Damage,"* 2nd ed., Gulf Professional Publishing, 2007.

[3] D. L. Wright, R. D. Watts, and E. Bramsoe, "A short-pulse electromagnetic transponder for hole-to-hole use," *IEEE Trans. Geosci. Remote Sens.,* Vol. GRS-22, No. 6, pp. 720–725, Nov. 1984.

[4] C. Guo and R. C. Liu, "A Borehole Imaging Method Using Electromagnetic Short Pulse in Oil-Based Mud," *Geosci. Remote Sens., Lett.* Vol. 7, No. 4, pp. 856–860, Oct. 2010.

[5] B. Panzner, A. Jostingmeier and A. Omar, "A compact double-ridged horn antenna for ground penetrating radar applications," 18th Int. Conf on Microwave Radar and Wireless Communications (MIKON), Vilnius, 2010, pp.1-4.

[6] G. F.J, S. G. Garcia, R. G. Martin, "GA design of a thin-wire bow-tie antenna for GPR applications," IEEE Trans. Geosci. Remote Sens., Vol.44, No.4, pp. 1004-1010, April 2006.

[7] A. S. Turk, "Ultra wideband TEM horn design for ground penetrating impulse radar system," Microwave *Optical Technology Lett.*, Vol. 41, No. 5, pp. 333–336, June 2004.

[8] J. A. G. Malherbe, N. Barnes, "TEM horn antenna with an elliptic profile," Microwave and Optical Technology Lett., Vol. 49, No. 7, 1548-1551, July 2007.

[9] P. R. Foster, J. D. Halsey, and M. G. M. Hussain, "Ultra-Wideband Antenna Technology," in Introduction to Ultra-Wideband Radar Systems, J. D. Taylor, Ed. Boca Raton, FL: CRC Press, 1995, Ch. 5.

[10] A. G. Yarovoy, A. D. Schukin, I. V. Kaploun, and L. P. Ligthart, "The dielectric wedge antenna," IEEE Trans. Antennas Propag., Vol. 50, No. 10, pp. 1460–1472, Oct. 2002.

[11] R. J.Wohlers, "The GWIA, an extremely wide bandwidth low-dispersion antenna," Buffalo, New York: Calspan Corporation, 1971.

[12] D. A. Kolokotronis, Y. Huang, and J. T. Zhang, "Design of TEM horn antennas for impulse radar," IEEE High Frequency postgraduate student colloquium, pp. 120–126, Sept 1999.

[13] A. R. Mallahzadeh and F. Karshenas," Modified TEM horn antenna for broadband applications," Progress In Electromagnetics Research, Vol. 90, PP. 105-119, 2009.

[14] L.L. Chen, C .Liao, L. Chang, X. Zheng, G. Su, J. Fang; , "A novel ultra-wideband knife-shape TEM horn antenna design for transient application, " Int. Conf. on Microwave and Millimeter Wave Technology (ICMMT), 2010, pp.355-358.

[15] C.Kyungho, S. Pyun, C. Jaehoon, "Design of an ultrawide-band TEM horn antenna with a microstrip-type balun," IEEE Trans. Antennas Propag., Vol.53, No.10, pp. 3410- 3413, Oct. 2005.

[16] D. Oloumi, M.I. Pettersson, D. Elliott, P. Mousavi, "A TEM Horn Antenna with Non-uniform Expansion for Oil Well Monitoring," accepted to be presented at antenna and propagation symposium, .Chicago, 2012.

[17] M. Skolnik, "Introduction to Radar Systems," 3rd Ed. New York: McGraw-Hill, 2001.

[18] L. E. Andresson, " On the determination of function from spherical averages," SIMA Journal on Mathematical Analysis, Vol. 19, No. 1, pp. 214-232, 1988.

Conclusion to the thesis

Oil well monitoring is very important for the oil and gas industry. Therefore in this thesis, a new ultra-wideband (UWB) ground penetrating radar (GPR) system for detection of near wellbore formation damage is introduced. The proposed GPR uses ground penetrating synthetic aperture radar (GPSAR) and a new developed transverse electromagnetic (TEM) horn antenna to increase GPR image resolution. The work has therefore been divided in two parts of synthetic aperture radar (SAR) processing of ground penetrating data and TEM horn antenna design as UWB transceiver for this system.

In the first part GPR data is processed with SAR to achieve better horizontal resolution. The results show that the combination of GPR and SAR is a good solution to achieve high resolution images in both range and cross range (directions of the oil well axis). This method is very beneficial in borehole radar imaging where use of a big antennas to achieve high resolution in cross range direction is not feasible.

In the second part of thesis, a TEM horn antenna is designed that fits into the oil well. A new profile for TEM horn antenna is introduced to remove the ripples and dips in antenna mainlobe radiation pattern which is normally a problem with this type of UWB horns. The designed antenna is simulated and fabricated and the measurement results fully verify the simulation results.

Future work will be on extracting materials electromagnetic properties like dielectric constant and loss tangent by invers scattering techniques from the recorded data by the GPSAR system. This work would be very interesting for companies who are working on geology and underground material investigation.

In future work the antenna design will be very important since the antenna is one of the most critical parts of UWB radar systems. Therefore, investigations of antenna impulse response enhancement and antenna performance estimation will be made.